Title
GGGGCC repeat expansion in C9orf72 compromises nucleocytoplasmic transport

Journal
Nature, 525(7567)

ISSN
0028-0836

Authors
Freibaum, Brian D
Lu, Yubing
Lopez-Gonzalez, Rodrigo
et al.

Publication Date
2015-09-01

DOI
10.1038/nature14974

Peer reviewed

HHS Public Access

Author manuscript

Nature. Author manuscript; available in PMC 2016 March 03.

Published in final edited form as:

Nature. 2015 September 3; 525(7567): 129–133. doi:10.1038/nature14974.

GGGGCC repeat expansion in *C9ORF72* compromises nucleocytoplasmic transport

Brian D. Freibaum[1,*], **Yubing Lu**[2,*], **Rodrigo Lopez-Gonzalez**[2], **Nam Chul Kim**[1], **Sandra Almeida**[2], **Kyung-Ha Lee**[1], **Nisha Badders**[1], **Marc Valentine**[1], **Bruce L. Miller**[3], **Philip C. Wong**[4], **Leonard Petrucelli**[5], **Hong Joo Kim**[1], **Fen-Biao Gao**[2,‡], and **J. Paul Taylor**[1,‡]

[1]Department of Cell and Molecular Biology, St. Jude Children's Research Hospital, Memphis, TN 38105, USA

[2]Department of Neurology, University of Massachusetts Medical School, Worcester, MA 01605, USA

[3]Memory and Aging Center, Department of Neurology, University of California San Francisco, San Francisco, CA 94158, USA

[4]Department of Pathology, The Johns Hopkins University School of Medicine, Baltimore, MD 21205-2196, USA

[5]Department of Neuroscience, Mayo Clinic Florida, Jacksonville, FL 3224, USA

Abstract

GGGGCC (G_4C_2) repeat expansion in a noncoding region of *C9ORF72* is the most common cause of sporadic and familial forms of amyotrophic lateral sclerosis (ALS) and frontotemporal dementia (FTD)[1,2]. The basis for pathogenesis is unknown. To capture the consequences of G_4C_2 repeat expansion in a tractable genetic system, we generated transgenic fly lines expressing 8, 28 or 58 G_4C_2 repeat-containing transcripts that do not have a translation start site (AUG) but contain an open-reading frame for green fluorescent protein (GFP) to detect repeat-associated non-AUG (RAN) translation. These transgenic animals show dosage-dependent, repeat length-dependent degeneration in neuronal tissues and RAN translation of dipeptide repeat (DPR) proteins as observed in patients. This model was used in a large-scale, unbiased genetic screen ultimately leading to the identification of 18 genetic modifiers that encode components of the nuclear pore complex (NPC) as well as the machinery that coordinates the export of nuclear RNA and the import of nuclear proteins. Consistent with these results we found morphological abnormalities in the architecture of the nuclear envelope in cells expressing expanded G_4C_2 repeats *in vitro* and *in*

‡Correspondence: J. Paul Taylor, MD. Ph.D. jpaul.taylor@stjude.org or Fen-Biao Gao, Ph.D. fen-biao.gao@umassmed.edu.
*These authors contributed equally to this work.

Online Content

Methods, along with any additional Extended Data display items and Source Data, are available in the online version of the paper; references unique to these sections appear only in the online paper.

Author Contributions

F.B.G. and J.P.T. conceived and supervised the project. B.D.F., Y.L., H.J.K, F.B.G. and J.P.T. wrote the manuscript. B.D.F. and Y.L. performed the genetic screen and validation. B.D.F., Y.L., N.C.K., N.B. and K.H.L. characterized *Drosophila* phenotypes and performed the assays characterizing RNA export in human cells. S.A. established human fibroblast cell lines, R.L.G. generated some iPS cell lines, S.A. and R.L.G. performed cortical neuron differentiation. M.V. and B.D.F. conducted FISH experiments. L.P. B.L.M. and P.W. provided key reagents.

vivo. Moreover, we identified a substantial defect in RNA export resulting in retention of RNA in the nuclei of *Drosophila* cells expressing expanded G_4C_2 repeats and also in mammalian cells, including aged iPSC-derived neurons from *C9ORF72* patients. These studies show that a primary consequence of G_4C_2 repeat expansion is the compromise of nucleocytoplasmic transport through the nuclear pore, revealing a novel mechanism of neurodegeneration.

Keywords

ALS; C9ORF72; DPR; *Drosophila*; FTD; genetic screen; nuclear pore; RAN translation; repeat expansion

To explore pathogenic mechanisms of disease initiated by *C9ORF72* repeat expansion in a genetically tractable model organism, we used PhiC31 integrase mediated insertion of 8, 28 or 58 copies of G_4C_2 repeats into specific genomic loci of *Drosophila*. These repeats are not expressed at baseline but are transcribed when GAL4 is introduced in *trans* by genetic cross (Fig. 1a). The GFP coding sequence without a start codon was placed in frame with a potential poly(GP) dipeptide repeat (Fig. 1a), although RAN translation of the sense strand may also occur in two other reading frames producing poly(GR) and poly(GA).

We expressed these constructs in the *Drosophila* eye using *GMR-GAL4* and observed a length- and dosage-dependent rough eye phenotype (Fig. 1b) similar to that reported recently[3,4]. Toxicity was also observed when these repeats were expressed in other tissues. Expression of G_4C_2-58, but not G_4C_2-8, in motor neurons using *OK371-GAL4* led to small larvae with significantly impaired locomotor activity (Fig. 1c, d). The neuromuscular junctions (NMJs) were examined with presynaptic and postsynaptic markers (Fig. 1e). Expression of G_4C_2-58 resulted in a significant decrease in bouton number and total muscle area when compared with GFP or G_4C_2-8 (Fig. 1f). Additionally, active zones within the NMJ were markedly reduced in larvae expressing G_4C_2-58 compared with controls (Extended Data Fig. 1a, b). Expression of G_4C_2-58 by the pan-neuronal driver *elav-GAL4* also resulted in dosage-dependent locomotor defects and NMJ abnormalities (Extended Data Fig. 1c–f). Moreover, expression of G_4C_2 repeats by the muscle-specific driver *MHC-GAL4* led to age-dependent defects in indirect flight muscle resulting in permanent abnormal wing position as compared to controls (Extended Data Fig. 1g).

In this fly model, RAN translation occurs in a G_4C_2 repeat length-dependent manner. Poly(GP)-GFP DPRs were detected in flies expressing G_4C_2-58 and to a lesser extent G_4C_2-28, but not in flies expressing equivalent levels of G_4C_2-8 (Extended Data Fig. 2a, b). Indeed, nuclear and cytoplasmic inclusions of poly(GP)-GFP were present in tissues expressing G_4C_2-58 but not G_4C_2-8 such as brain, muscle and salivary gland cells (Extended Data Fig. 2c–g). To determine whether DPRs are sufficient to drive a degenerative phenotype, we used codons alternate to G_4C_2 to generate new transgenic flies directly expressing poly(GA), poly(GR), or poly(GP), with an AUG start codon and N-terminal GFP (Supplementary Table 1; Extended Data Fig. 3a). Expression of neither GFP-$(GP)_{47}$ nor GFP-$(GA)_{50}$ elicited a degenerative eye phenotype (Extended Data Fig. 3a, b). Thus, while poly(GP)-GFP serves as a useful marker of cells expressing G_4C_2-58 RNA and producing DPR proteins, it is unlikely to contribute significantly to the degenerative phenotype. By

contrast, expression of GFP-$(GR)_{50}$ was highly toxic resulting in greater than 95% lethality with a few escapers having severely degenerated eyes (Extended Data Fig. 3a). These results are consistent with recent reports indicating that poly(GR) is toxic in cultured cells and *Drosophila*[3,5,6]. In fact, immunoblotting with antibodies against DPRs showed that flies expressing G_4C_2-58 RNA produce poly(GR) in addition to poly(GP) DPRs, although neither poly(GA) nor poly(PR) was detected (Extended Data Fig. 3c, d). Thus, G_4C_2-58 toxicity may be mediated through toxic RNA or poly(GR) produced in our fly model, or a combination of these mechanisms.

To gain unbiased insight into the pathogenic mechanisms underlying G_4C_2-58 toxicity, we performed a large-scale genetic screen to identify genetic loci whose partial loss of function may significantly modify the G_4C_2-58-induced rough eye phenotype. To this end, flies expressing G_4C_2-58 in the eye were crossed with 372 chromosomal deficiency lines spanning the entirety of the 2nd and 3rd chromosomes, representing ~80% of the fly genome. In total, 5.1% of the deficiencies were found to suppress the rough eye phenotype whereas 8.8% of these enhanced the rough eye phenotype (Extended Data Table 2).

Two deficiency lines on the 2nd chromosome, *Df(2R)1725* and *Df(2R)1735*, each in heterozygotes had no eye phenotype by themselves but led to a marked enhancement of the G_4C_2-58 rough eye phenotype (Fig. 2a). The genomic regions covered by these deficiencies partially overlap (Fig. 2b), suggesting one or more genes in this overlapping region are responsible for the observed enhancement. After systematic evaluation of this candidate interval with classical loss of function (LOF) alleles and RNAi lines, we identified the gene *Nup50*, whose partial LOF enhanced the G_4C_2-58 phenotype (Fig. 2c). The effect of the *Nup50* was specific to G_4C_2-58 since there was no rough eye phenotype present when *Nup50* was knocked down in eyes expressing GFP (Fig. 2c). Nup50 is a component of the nuclear pore and also plays a critical role in promoting protein nuclear import through interaction with Importin β and Ran GTPase[7], Consistent with the impact of *Nup50* LOF on G_4C_2-58-mediated degeneration, a dominant-negative form of Ran (Ran^{T24N})[8] strongly enhanced the G_4C_2-58 rough eye phenotype (Extended Data Fig. 4a). Moreover, the nuclear import factors Nup153 and Transportin, which work in concert with Nup50 and Ran[7], were also identified as enhancers of the G_4C_2-58 rough eye phenotype (Extended Data Fig. 4a). These genetic analyses suggest that protein import is compromised by G_4C_2-58 expression.

The strongest suppressor identified in the genetic screen was *Ref1*, revealed by interrogation of the suppressor deficiency *Df(3R)Antp17* (Fig. 2d, e). This deficiency also suppressed the strong rough eye phenotype produced by two copies of G_4C_2-58, as did heterozygosity for the null allele $Ref1^{02267}$ (Fig. 2f). *Ref1*, and its human ortholog *ALYREF*, are RNA-binding proteins that associate with the 5′ end of mRNAs to prevent degradation by the nuclear exosome and, together with the TREX component CHTOP, facilitate delivery of fully processed mRNAs to the nuclear pore receptor NXF1 that mediates their export through the nuclear pore[9–12]. Consistent with the impact of *Ref1* LOF on G_4C_2-58-mediated degeneration, partial LOF of *NXF1* or *CHTOP* enhanced the rough eye phenotype (Fig. 2g, h, Extended Data Fig. 5). The fact that the G_4C_2-58 phenotype is exacerbated by LOF in *NXF1* or *CHTOP*, but partially rescued by LOF of *Ref1* perhaps highlights the dual role played by *Ref1* in partitioning target RNAs between the nuclear pore and the nuclear

exosome[9]. Indeed, in support of this interpretation we identified LOF in *EXOSC3* and *EXOSC10*, which encode components of the nuclear exosome, as strong enhancers of G_4C_2-58-related toxicity (Fig. 2g, h, Extended Data Fig. 5). Notably, LOF mutations in *EXOSC3* in humans cause a congenital form of motor neuron disease[13].

The genes encoding cap-binding proteins NCBP1, NCBP2, and ARS2, that mediate recruitment of the TREX complex to the 5′ end of RNA to initiate RNA export[14], were also identified as enhancers of G_4C_2-58-mediated degeneration (Fig. 2g, h, Extended Data Fig. 5). Moreover, we found that LOF of either *Nup107* or its binding partner *Nup160*, both of which are nuclear pore components responsible for exporting some RNAs[15–17], suppressed the G_4C_2-58 rough eye phenotype (Extended Data Fig. 5). One particularly notable enhancer was the *Drosophila* ortholog of human *GLE1*, a critical mediator of RNA export at the nuclear pore[18] (Fig. 2g, h, Extended Data Fig. 5). Interestingly, complete LOF of human *GLE1* causes congenital motor neuron disease[19], whereas partial LOF of human *GLE1* is associated with adult-onset ALS[20].

The identification of TREX and nuclear pore proteins as genetic modifiers strongly implies that not only is nuclear import compromised by G_4C_2-58 expression, but also nuclear export of RNAs and proteins. Consistent with this latter notion we found that LOF of *Crm1*, a gene encoding a major receptor for the export of RNAs and proteins, resulted in significant enhancement of the G_4C_2-58 phenotype (Extended Data Fig. 4b). Moreover, expression of G_4C_2-58 in motor neurons caused exquisite sensitivity to leptomycin B, an inhibitor of nuclear export (Extended Data Fig. 4c). In total, the genetic screen and follow up analyses identified 18 modifier genes within the pathway of nucleocytoplasmic transport, and RNA export in particular, highlighting this system as an important target of G_4C_2-58-related toxicity (Fig. 2g, h, Supplementary Table 3). In particular, the identification of 4 strong suppressors of G_4C_2-58 indicates that compromised nucleocytoplasmic transport is an important causal pathway responsible for degeneration.

In follow up to our genetic studies, RFP-Nup107 was expressed in salivary glands using *Fhk-GAL4*. In cells expressing G_4C_2-8, Nup107 labels a distinct nuclear boundary that is morphologically indistinguishable from cells expressing GFP (Fig. 3a). In contrast, in cells expressing G_4C_2-58, the nuclear envelope exhibited a wrinkled appearance and in many nuclei, Nup107 was found to form inclusions near the nuclear envelope (Fig. 3a). To further explore nuclear architecture, the nuclear envelope was visualized by immunostaining of endogenous Lamin C. 43.7% of cells expressing G_4C_2-58 showed an abnormal, “frayed” nuclear envelope phenotype, whereas this phenotype was observed in only 7.1% of cells expressing G_4C_2-8 (Fig. 3b, c, Extended Data Fig. 6a). Thus, G_4C_2-58 expression causes defects in the architecture of the nuclear envelope and mislocalization of nucleoporins. Moreover, cells expressing one copy of G_4C_2-58 showed a significant increase in the ratio of nuclear to cytoplasmic RNA in comparison to cells expressing GFP or G_4C_2-8 (Fig. 3d, e). Expression of 2 copies of G_4C_2-58 resulted in a more pronounced retention of nuclear RNA (Fig. 3d, e). Importantly, depletion of *Ref1* by RNAi partially suppressed the nuclear RNA retention phenotype in cells expressing G_4C_2-58, reducing nuclear RNA density to control levels (Fig. 3d, e). Thus, G_4C_2 length-dependent degeneration in *Drosophila* is accompanied by nuclear retention of RNA, consistent with the results of the unbiased genetic screen.

Similar retention of nuclear RNA was observed in HeLa and HEK293T cells upon transient expression of G_4C_2-58, but not G_4C_2-8 (Fig. 4a–e, Extended Data Fig. 6b). Specifically, this export defect was illustrated using an alternate approach to monitor the fate of newly synthesized RNA by metabolic labeling. In HeLa cells expressing G_4C_2-58, we observed a significant decrease in the export of nascent RNA in comparison to control cells expressing GFP or G_4C_2-8, although the total levels of metabolically labeled transcripts were comparable (Fig. 4a–c, Extended Data Fig. 6c). Moreover, polyA$^+$ mRNA as detected by an oligo-dT probe accounts for at least some portion of the retained RNA in mammalian cells expressing G_4C_2-58 (Fig. 4d, e).

Advances in induced pluripotent stem (iPS) cell technology permit the generation of neurons from patients including those with FTD and ALS[21]. To further examine the impact of expanded G_4C_2 toxicity on nucleocytoplasmic transport in a more relevant human cell type from *C9ORF72* patients, we examined the subcellular distribution of total RNA in 2-month-old cortical neurons, which are affected in FTD, a frequent clinical feature of *C9ORF72*-related disease[22]. These neurons were differentiated from previously characterized[23–25] as well as newly generated and characterized iPS cell lines derived from 5 *C9ORF72* patients and 3 controls (Extended Data Figs. 7 and 8, Supplementary Tables 4 and 5). Consistent with our observations in fly, HEK293T and HeLa cells, this analysis confirmed a significant increase in the nuclear to cytoplasmic ratio of RNA in *C9ORF72* patient cells in comparison to controls (Fig. 4f, g). On average, *C9ORF72* neurons showed a 35% increase in the nuclear to cytoplasmic ratio of RNA density (Fig. 4g). Interestingly, this difference in the ratio of nuclear to cytoplasmic RNA was not observed in fibroblasts obtained from *C9ORF72* patients when compared to controls, consistent with low levels of *C9ORF72* expression in fibroblasts[25] (Extended Data Fig. 9a–c). Thus, neurons derived from patients with *C9ORF72*-related disease mirror the nucleocytoplasmic transport defects identified by unbiased approaches in a genetic model of disease.

The NPC is the largest macromolecular complex in eukaryotic cells, consisting of multiple copies of more than 30 different proteins[26]. Some structural components of the NPC have an exceedingly long half-life measured in years[27]. Indeed, nuclear pores are a particularly intriguing target for age-related diseases affecting post-mitotic cells such as neurons, putting them at risk of accumulating damage over extended periods of time[27]. Nucleocytoplasmic transport through the nuclear pore is vital to cell viability, and primary defects in this function cause of a host of human diseases of varying phenotypes ranging from cancer to neurological disease[26,28,29].

Important questions regarding the pathogenesis of *C9ORF72*-related disease remain; in particular the relative contribution of expanded G_4C_2 RNA vs. DPRs or other mechanisms, which could cause the nuclear pore defect. Also to be determined is whether defects in nucleocytoplasmic transport and other reported defects such as sequestration of specific RNA binding proteins, nucleolar stress and ER stress are parallel processes or directly connected with each other. The rapid pace of discovery in this area of disease biology suggests that answers to these questions will come soon.

Methods

Generation of *Drosophila* lines

To generate transgenic *Drosophila* expressing G_4C_2-8, G_4C_2-28 and G_4C_2-58, G_4C_2 repeats of the respective length were cloned downstream of the UAS promoter and upstream of the EGFP sequence with the start codon removed in the plasmid pUAST-ATTB. Transgenic *Drosophila* lines were generated by BestGene Inc. such that the transgene was inserted using the PhiC31 integrase into either the attP2 site on chromosome 3 (loci 68A4) or the attP40 site on chromosome 2 (loci 25C6). GFP-$(GP)_{47}$, GFP-$(GA)_{50}$, and GFP-$(GR)_{50}$ plasmids[30] were subcloned into the pUAST-ATTB plasmid and inserted into the attP2 site by BestGene Inc. Flies were raised at 25°C on a standard diet. A complete listing of *Drosophila* stocks that modify the G_4C_2-58 phenotype are listed in Supplementary Table 3. For genetic interaction studies, the combined stock (*GMR-GAL4/Cyo; UAS-G_4C_2-58/Tm6,Tb*) was crossed with deficiency stocks or individual mutants and phenotypic analysis was performed on flies aged 24–48 hours in both males and females. Knock down efficiency of RNAi lines was measured by quantitative RT-PCR (Extended Data Fig. 10, Supplementary Table 6). For nuclear envelope morphology studies, the recombined stocks (*Fkh-GAL4, UAS-GFP/TM6,Tb; Fkh-GAL4, UAS-G_4C_2-8/TM6,Tb*; and *Fkh-GAL4,UAS-G_4C_2-58/TM6,Tb*) were crossed with *UAS-mRFP-Nup107* transgenic flies or immunostained for endogenous Lamin C.

Drosophila stocks

Deficiency stocks were obtained from the Bloomington *Drosophila* Stock Center deficiency kit. RNAi lines were obtained from either the Bloomington *Drosophila* Stock Center or the Vienna *Drosophila* RNAi Center. *UAS-RAN^{T24N}* and *Fkh-Gal4* flies were kindly provided by Drs. K. S. McKim and E. Baehrecke respectively.

Drosophila eye, muscle and neuronal phenotype analysis

Phenotypic analysis of G_4C_2 repeat expression in the *Drosophila* eye, muscle, and salivary gland was assessed by crossing G_4C_2-8, G_4C_2-28 and G_4C_2-58 lines to *GMR-GAL4, MHC-GAL4*, and *FKH-GAL4*, respectively. Neuronal expression was achieved by crossing G_4C_2-8, G_4C_2-28 and G_4C_2-58 lines to *elav-GAL4* (pan neuronal driver) or *OK371-GAL4* (motor neuron driver). Eye phenotypes were imaged by light microscopy and muscle phenotypes were visually assessed by wing posture (n=30 controls, 21 G_4C_2-8, 50 G_4C_2-28 and 24 G_4C_2-58). Neuromuscular synaptic bouton number, active zone density and crawling ability were measured as previously described[31,32] with slight modification. To count type 1b synaptic bouton number, each genotype was double stained presynaptically with anti-HRP-Cy3 (1:200, Jackson Immunoresearch) and postsynaptically with anti-Disc large 1 (1:50, DSHB). Synaptic boutons of muscle 4 in abdominal segment 2, 3 and 4 (A2–A4) were imaged with a Marianas spinning disc microscope and maximum projection images were used to count synaptic boutons. Active zone area and presynaptic area stained by anti-Bruchpilot (NC82, 1:100, DSHB) and anti-HRP-Cy3 were measured with ImageJ and the ratio of active zone area/presynaptic area was calculated. Muscle 4 in abdominal segment 2, 3 and 4 (A2–A4) was analyzed. To examine crawling ability, 4–7 wandering 3rd instar larvae for each group were collected, washed and placed onto a 3% agarose gel in a 10 cm dish.

After 5 min acclimation, larval crawling behavior was recorded by a digital camera for 30 sec (15 fps). Each group was tested three times. Moving distances of each larva were manually measured with ImageJ.

Immunofluorescence analysis of salivary gland cells

Dissected salivary glands from wandering third instar larvae were fixed with 4% paraformaldehyde (PFA) at room temperature for 15 min, washed three times with phosphate-buffered saline (PBT, 0.1% Triton X-100 in PBS), and blocked for 1 hr at room temperature with 10% normal goat serum (Sigma) diluted in PBT. Tissues were then incubated overnight at 4°C with mouse anti-Lamin C (1:30, LC28.26; Developmental Studies Hybridoma Bank (DSHB)). After three washes in PBT (10 min each), Tissues were incubated for 1 hr at room temperature with secondary antibodies (goat anti-mouse Alexa Fluor 568, 1:200; Invitrogen) diluted in the blocking solution. Tissues were washed three times in PBS and mounted with VECTASHIELD (Vector Laboratories). Fluorescence signals were examined with an Olympus IX70 Microscope or Leica TCS SP5 II laser scanning confocal microscope.

Visualization of RAN products in muscle cells

To visualize poly(GP)-GFP in the thorax expressing G_4C_2-58, flies were cleared overnight using a modified ScaleA2 (2 M urea, 10% glycerol, 0.1% Triton-X). RAN peptides were visualized using light sheet microscopy. To visualize RAN products at high magnification, thoraxes were dissected and stained with the same immunofluorescence protocol described above for salivary glands but using anti-Lamin (1:100, ADL 67.10; Developmental Studies Hybridoma Bank (DSHB)) to visualize the nucleus and phalloidin (1:40, Life Technologies) to visualize the muscle structure.

Immunoblots

Adult flies were frozen with dry ice and vortexed to remove the heads or thorax. Samples from each genotype were homogenized in RIPA buffer with proteinase inhibitor cocktail added. Urea buffer (7 M urea, 2 M thiourea, 4% CHAPS, 30 mM Tris pH8.5) was used when indicated to visualize the non-RIPA soluble protein fraction. Sample was mixed with 4X sample buffer (1 M Tris-HCl [pH 6.8], 8% SDS, 40% glycerol, 0.1% bromophenol blue) and boiled for 5 min, separated on a SDS gel and transferred to a membrane. The membrane was blocked, probed with primary antibody, and incubated with secondary antibody. The signal was visualized with either chemiluminescent substrate (SuperSignal West Pico; Pierce) or by using an Odyssey Fc (Li-Cor). Primary western blot antibodies were anti-GFP (AB3080, Millipore or SC-9996 Santa Cruz Biotechnology), anti-poly(GP), poly(GA) or poly(GR) antibodies[33,34], anti-β-actin antibody (4967; Cell Signaling Technology) or anti-actin antibody (sc-1616, Santa Cruz Biotechnology).

RNA *in situ* hybridization

Fixation of dissected salivary glands, cortical neurons, HeLa, or 293T cells (obtained from ATCC) was performed using 1% paraformaldehyde on ice for 5 min, followed by a second fixation in 1% paraformaldehyde plus 0.05% NP40 for an additional 5 min. Samples were

then transferred to 70% ethanol and stored at −20°C until needed. The probes for global RNA in either *Drosophila* or human cells were prepared from genomic DNA derived from w^{1118} flies or 293T cells. Both probes were labeled by nick translation using either alexafluor 594 dUTP. To hybridize the probes, 70 ng of the labeled probes (the human probe was combined with 2 μg of human cot1 DNA) were suspended in 10 μl of hybridization buffer consisting of 50% formamide, 2X SSC, and 10% dextran sulfate. Fixed cells were dehydrated in 70%, 80%, and 100% ethanol for 2 min each prior to hybridization. Probes suspended in hybridization buffer were denatured at 70°C for 5 min and then applied to the dehydrated cells and hybridized at 37°C overnight. Samples were washed following hybridization in 50% formamide, 2X SSC at 37°C for 5 min, then briefly rinsed in room temperature PBS and mounted on slides with DAPI. To detect poly(A) mRNA, HeLa cells were fixed with 4% paraformaldehyde followed by ice cold methanol and 70% ethanol for 10min each. The cells were treated with 1 ng/ l μL of 5′-labeled Cy3-oligo-dT(20) at 37°C for 1 h. Samples were washed in room temperature PBS and mounted on slides with DAPI. Images were captured using either widefield fluorescence microscopy or a Marianas spinning disc microscope. An extended depth of focus function was used to combine all components of individual microscope fields.

Pulse-chase of newly synthesized RNA

HeLa cells were transfected with plasmids expressing GFP, G_4C_2-8 or G_4C_2-58 that had been subcloned into pcDNA 3.1 using Fugene HD (Promega). After 48 h incubation, cells were treated with to 1 mM 5-ethynyl uridine (EU) was for 1 h. RNA was then visualized at indicated time points using the Click-iT detection kit (Invitrogen) as recommended by the manufacturer. To visualize GFP signal, cells were co-stained using monoclonal anti-GFP (SC-9996, Santa Cruz Biotechnology) as a primary antibody.

iPSC lines

iPSC lines from 2 control subjects and 4 G_4C_2 repeat expansion carriers have been previously characterized[23–25,35] (please see Extended Data Table 4). Generation of integration-free induced pluripotent stem cells (iPSCs) from fibroblasts of one G_4C_2 expansion carrier and one control subject, using episomal plasmids with the reprogramming factors Oct4, Sox2, Klf4, Lin28 and L-Myc were performed as described before[36], which was approved by the University of Massachusetts Medical School Institutional Biosafety Committee. The use of human fibroblasts was approved by the UCSF Institutional Review Board and informed consent was obtained from all subjects. After reprogramming, characterization of iPSCs shows that cells have normal karyotype, express pluripotent markers and have the capacity to differentiate into cells of the three germ layers as described in Almeida et al., (2012, 2013)[23,35]. All the iPSC lines used here were tested regularly with no mycoplasma contamination.

Cortical neuronal cultures

4 iPSC lines from 3 control subjects and 6 iPSC lines from 5 *C9ORF72* carriers were differentiated to cortical neurons as described earlier[23,35] (please also see Extended Data Table 5). Neuronal cultures were aged for 8-weeks before fixation for RNA FISH.

Immunostaining for iPSCs and iPSCs-derived neurons

For immunostaining cells were fixed in 4% paraformaldehyde for 15 minutes and then permeabilized with 0.3 % Triton X-100 for 5 minutes. Cells were blocked with 5% bovine serum albumin for 30 minutes; cells were incubated with primary antibodies overnight at 4 °C. The following primary antibodies were used: mouse anti-OCT4 1:100 (Santa Cruz Biotechnology), goat anti-NANOG 1:100 (R&D Systems), mouse anti-SSEA4 1:100 (Abcam), rabbit anti-desmin 1:100 (Thermo Scientific), mouse anti-βIII-tubulin 1:500 (Promega), mouse anti-α-fetoprotein 1:200 (R&D Systems), mouse anti-MAP2 1:500 (Sigma), goat anti ChAT 1:200 (EMD Millipore), rabbit anti-VGLUT1 1:500 (Synaptic Systems). After incubation with primary antibodies cells were washed with PBS three times and incubated with Alexa Fluor secondary antibodies 1:500 (Invitrogen) for 1 h at room temperature followed by counter staining with DAPI.

Fluorescence *in situ* hybridization

FISH in iPSCs derived from control and *C9ORF72* expansion carrier using a Cy3-conjugated $(GGCCCC)_4$ probe was performed as described in Almeida et al., (2013)[23].

Quantification

For salivary glands, 30 cells from at least 5 individual salivary glands for each genotype were used for quantitative analysis. ImageJ software was used to measure the ratio of nuclear to cytoplasmic RNA by comparing the total RNA measured in the nucleus to that of the cytoplasm. DAPI was used to mark the nucleus. For cortical neurons, the ratio of nuclear to cytoplasmic RNA density was calculated by measuring the density of the RNA signal in both the nucleus and cell body using ImageJ software. DAPI was used to mark the nuclear boundary of neurons. For cortical neurons, at least 15 neurons were measured from each individual patient (Controls 1–3 (n=16, 16, 31) and Patients 1–5 (n=16,16,16,30,15)). Error bars for all quantification are standard error.

Extended Data

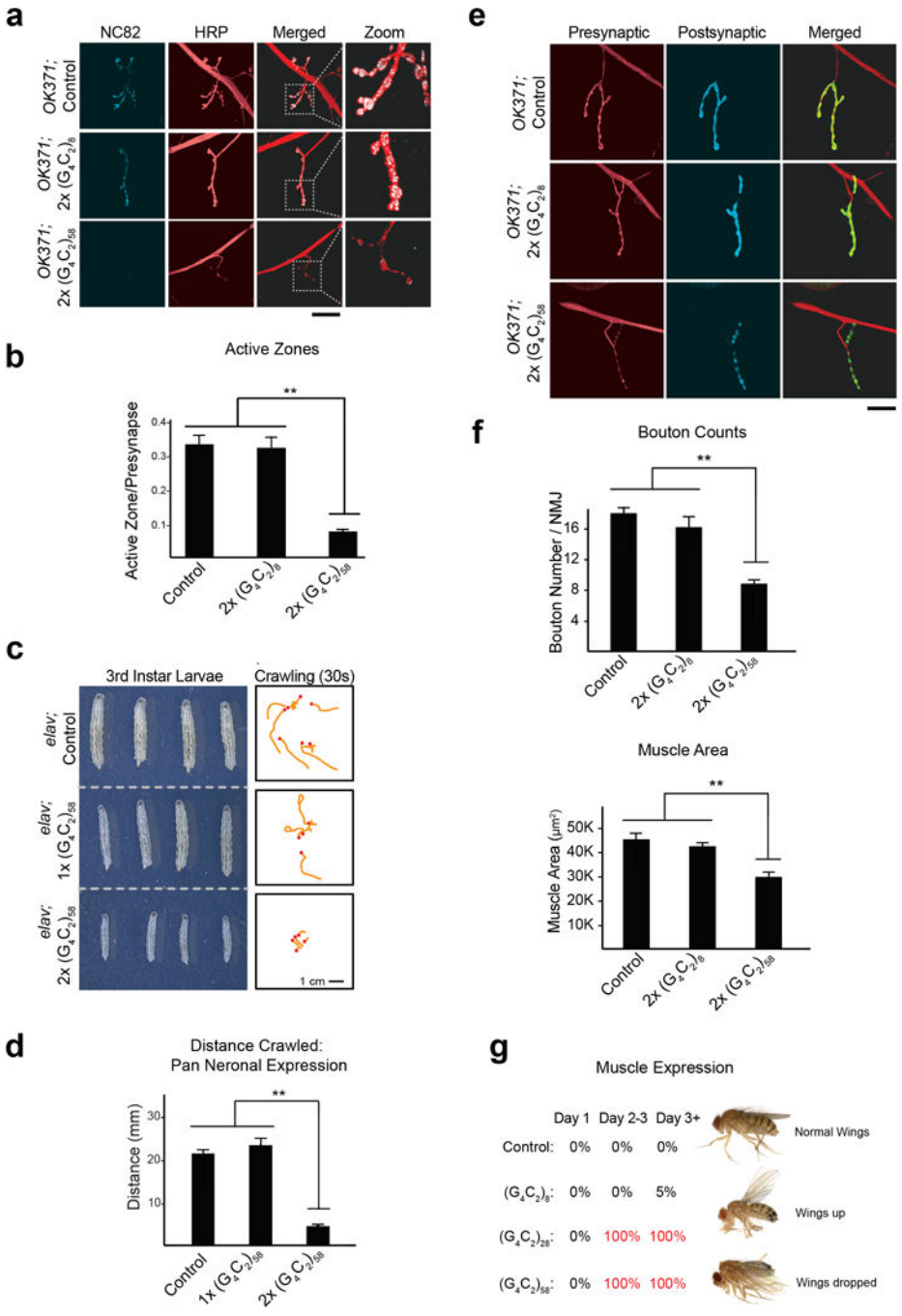

Extended Data Figure 1. Expression of G_4C_2 repeats induces length-dependent phenotypes in *Drosophila*

a, G_4C_2 *Drosophila* motor neurons using the *OK371-GAL4* driver leads to a significant reduction in active zones as immunostained by the anti-Bruchpilot antibody NC82 and anti-HRP. Scale bar: 50 μm. **b**, Quantification of active zones. Values are mean ± s.e.m. ** $p < 0.01$, One way ANOVA, Tukey's Post Hoc test. **c**, Pan Neuronal expression of G_4C_2-58 repeats induces dosage-dependent decrease in larval size (left) and locomotor activity

measured in 30 seconds (right) when G_4C_2-58 is expressed in all neurons using the *elav-GAL4* driver. **d**, Quantification of the distance traveled by third instar larvae reveals expressing two copies of G_4C_2-58 results in a significant deficit in locomotor activity. Values are mean ± s.e.m. n=3 trials, more than 4 larvae per group in each trial. ** $p < 0.01$, One way ANOVA, Tukey's Post Hoc test. **e**, Pan Neuronal expression of G_4C_2-58 repeats in Drosophila neurons using the *elav-GAL4* driver leads to a significant reduction in the bouton number. Bouton number was quantified by examining the presynaptic (anti-HRP) and postsynaptic (anti-DLG1) markers (left). Scale bar: 50 μm. **f**, Quantification of buoton number (left) and muscle size (right) reveal both are significantly reduced in *Drosophila* larvae expressing G_4C_2-58 repeats. Values are mean ± s.e.m. $n \geq 5$, ** $p < 0.01$, One way ANOVA, Tukey's Post Hoc test. **g**, Expression of G_4C_2-28 and G_4C_2-58 but not G_4C_2-8 in the muscle using the *MHC-GAL4* driver leads to loss of wing control in adult flies ($n > 20$ for all genotypes). This phenotype was assessed by examining the permanent wing posture of live adult flies.

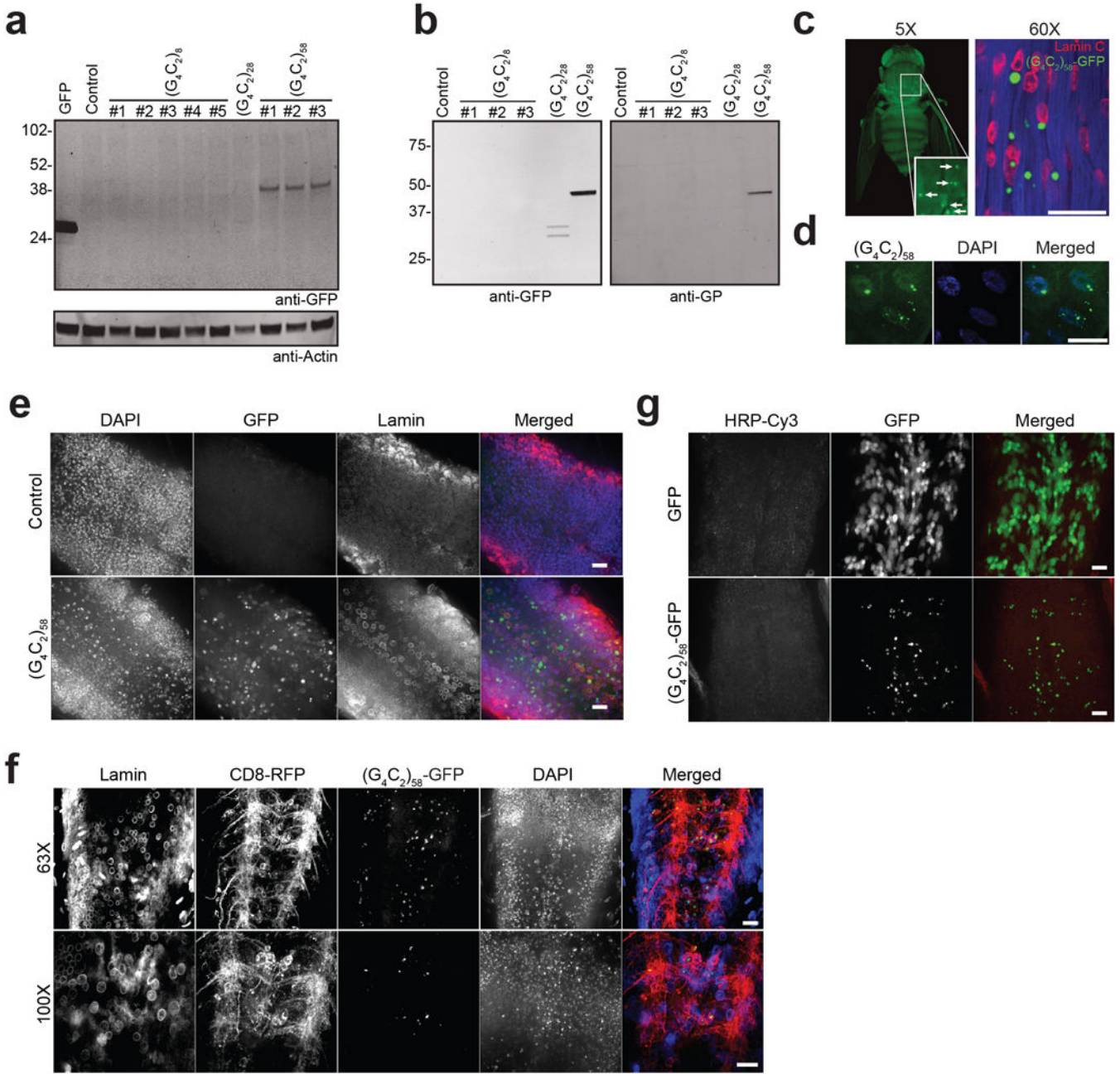

Extended Data Figure 2. RAN translation is observed in the *Drosophila* expressing G_4C_2 repeats

a, Western blot revealing translation of RAN poly-dipeptides in flies expressing G_4C_2-58 in the eye. RAN poly-dipeptides were not found in flies expressing G_4C_2-8 or control flies. There was minimal expression of GFP positive product observed in flies expressing G_4C_2-28. GFP expressing flies (lane 1) were used as a positive control for the anti-GFP antibody. **b**, Western blot showing production of RAN product when G_4C_2-28 and G_4C_2-58 but not G_4C_2-8 repeats are expressed in the muscle. RAN products were visualized with anti-GFP antibody (left) and anti-poly(GP) antibody (right). **c**, The RAN product poly-GP-GFP from flies expressing G_4C_2-58 in the muscle form large visible inclusions as visualized under light sheet fluorescent microscopy (left) and by confocal microscopy (right). Scale

bar: 50 μm. **d**, Expression of G_4C_2-58 in the salivary gland cells results in the formation of large nuclear inclusions and smaller cytoplasmic inclusions. Scale bar 50 μm. **e–f**, Expression of G_4C_2-58 in the ventral ganglion by *OK371* driver results in the formation of nuclear and cytoplasmic inclusions, whereas GFP shows diffused nuclear and cytoplasmic localization. Lamin staining shows nuclear membrane, and CD8-RFP shows plasma membrane. Scale bars: 25 μm. **g**, Expression of G_4C_2-58 in pan neuronal cells by *elav* driver results in the nuclear and cytoplasmic inclusions. Scale bar: 25 μm.

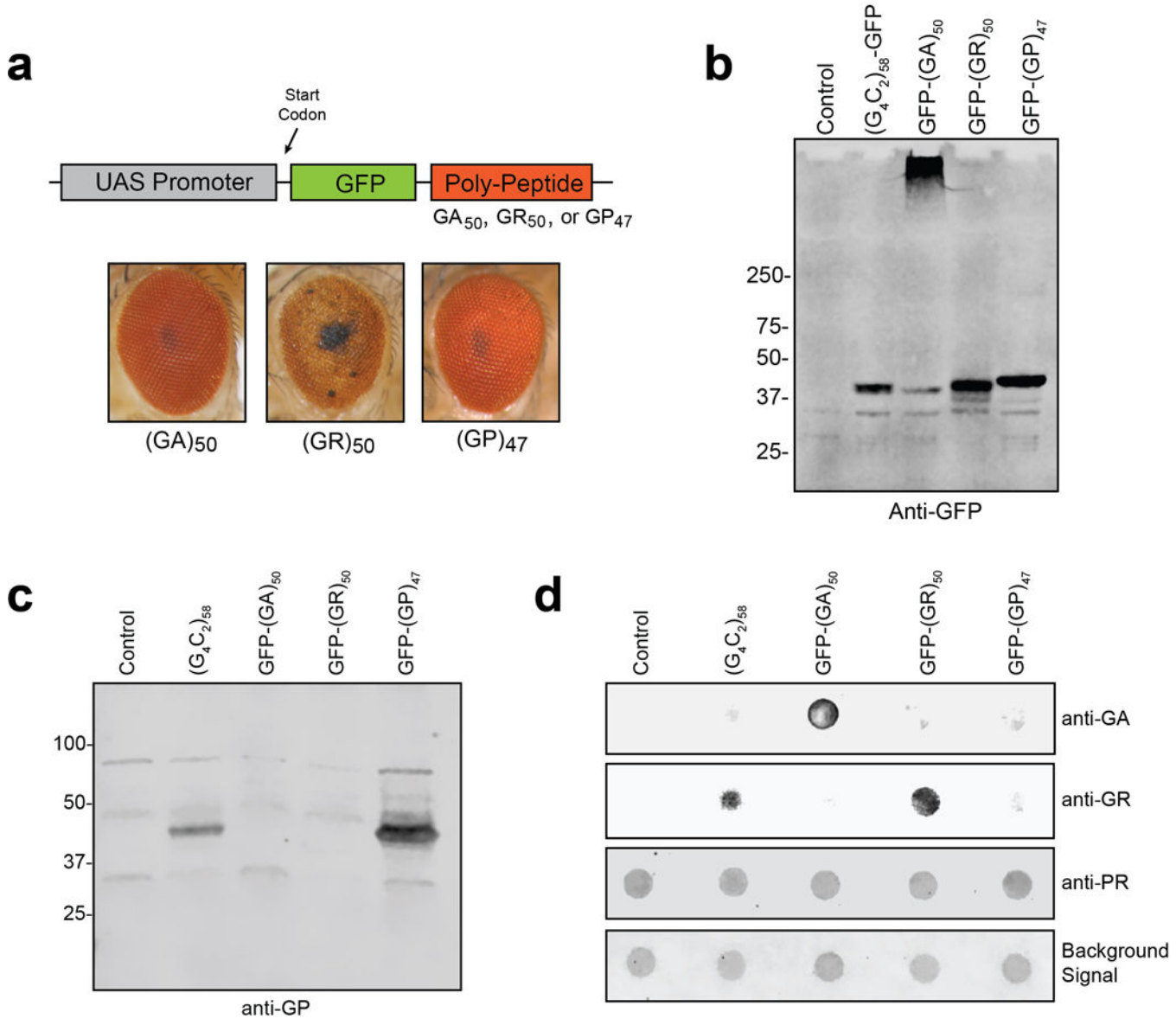

Extended Data Figure 3. Ectopic expression of poly(GR) but not poly(GA) or poly(GP) peptides are toxic in *Drosophila*

a, Transgenic *Drosophila* were generated that express ATG driven poly(GA), poly(GR) and poly(GP) peptides with an N-terminal GFP tag (top). Expression of GFP-(GA)50 and GFP-(GP)47 were nontoxic when expressed in the eye with GMR-GAL4 whereas GFP-(GR)50

expression resulted in >95% lethality with surviving adults having severely degenerated eyes (bottom). **b**, Western blot showing the expression of G_4C_2-58, GFP-(GA)50, GFP-(GR)50 and GFP-(GP)47 as visualized in muscle by anti-GFP antibody. **c**, Western blot showing the expression of poly(GP) in muscle of flies expressing G_4C_2-58 and GFP-(GP)47 but not GFP-(GA)50, GFP-(GR)50 and control flies as visualized by anti-GP antibody. **d**, Dot blot analysis of RAN peptides in muscle revealing expression of poly(GA) only in GFP-(GA)50 flies, expression of poly(GR) in G_4C_2-58 and GFP-(GR)50 flies. As expected, anti-sense DPR poly(PR) was not found in any of the lysates. The background protein signal was used as a loading control.

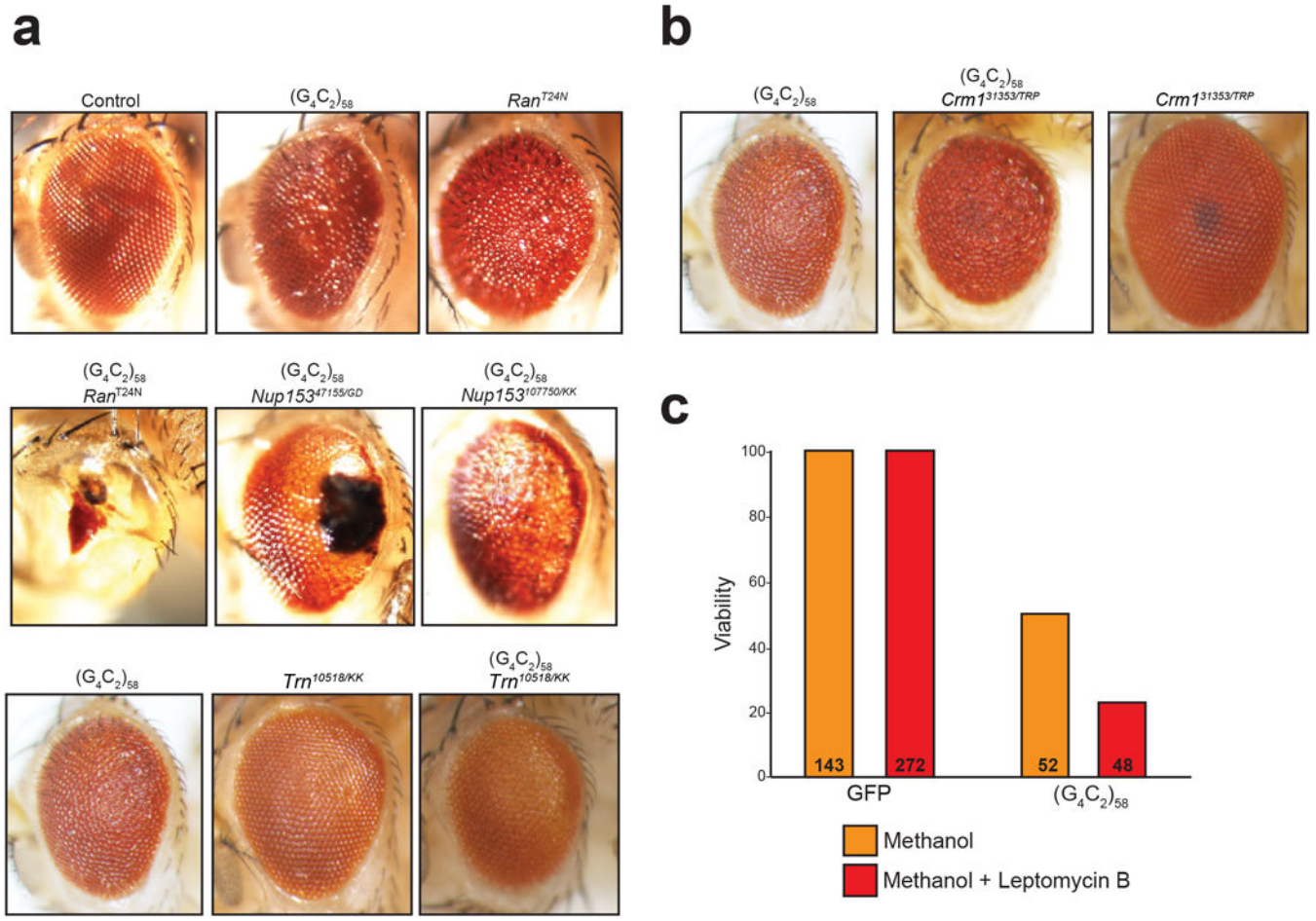

Extended Data Figure 4. Nuclear import and export is altered by G_4C_2-58 expression

a, A threonine to asparagine substitution at residue 24 in the Ran protein abolishes the affinity for GTP and reduces its affinity for GDP. Hence, the Ran (T24N) is always in either a nucleotide free state or in its inactive, GDP-bound state, and acts as dominant negative. RANT24N expression driven by GMR-GAL4 causes a mild eye phenotype when expressed in the absence of G_4C_2-58 (upper row, right panel). The G_4C_2-58 rough eye phenotype is strongly enhanced by dominant negative RANT24N expression (middle row, left panel). The G_4C_2-58 eye phenotype is significantly enhanced by knockdown of Nup153 by two independent RNAi lines (middle row, two right panels). The G_4C_2-58 eye phenotype is also

mildly enhanced by knockdown of transportin (Trn) (bottom row). **b**, Knockdown of Crm1 in flies expressing G_4C_2-58 induces a mild enhancement of the G_4C_2-58 eye phenotype (left vs. middle). Crm1 knockdown in the absence of G_4C_2-58 repeats does not produce a rough eye phenotype (left). **c**, Expression of two copies of G_4C_2-58 in the *Drosophila* motor neurons leads to reduced viability (50%). Chemical inhibition of Crm1 with Leptomycin B (500 nM) enhances G_4C_2-58 toxicity resulting in reduced viability (23%). Leptomycin B does not impede viability (100%) in *Drosophila* expressing GFP.

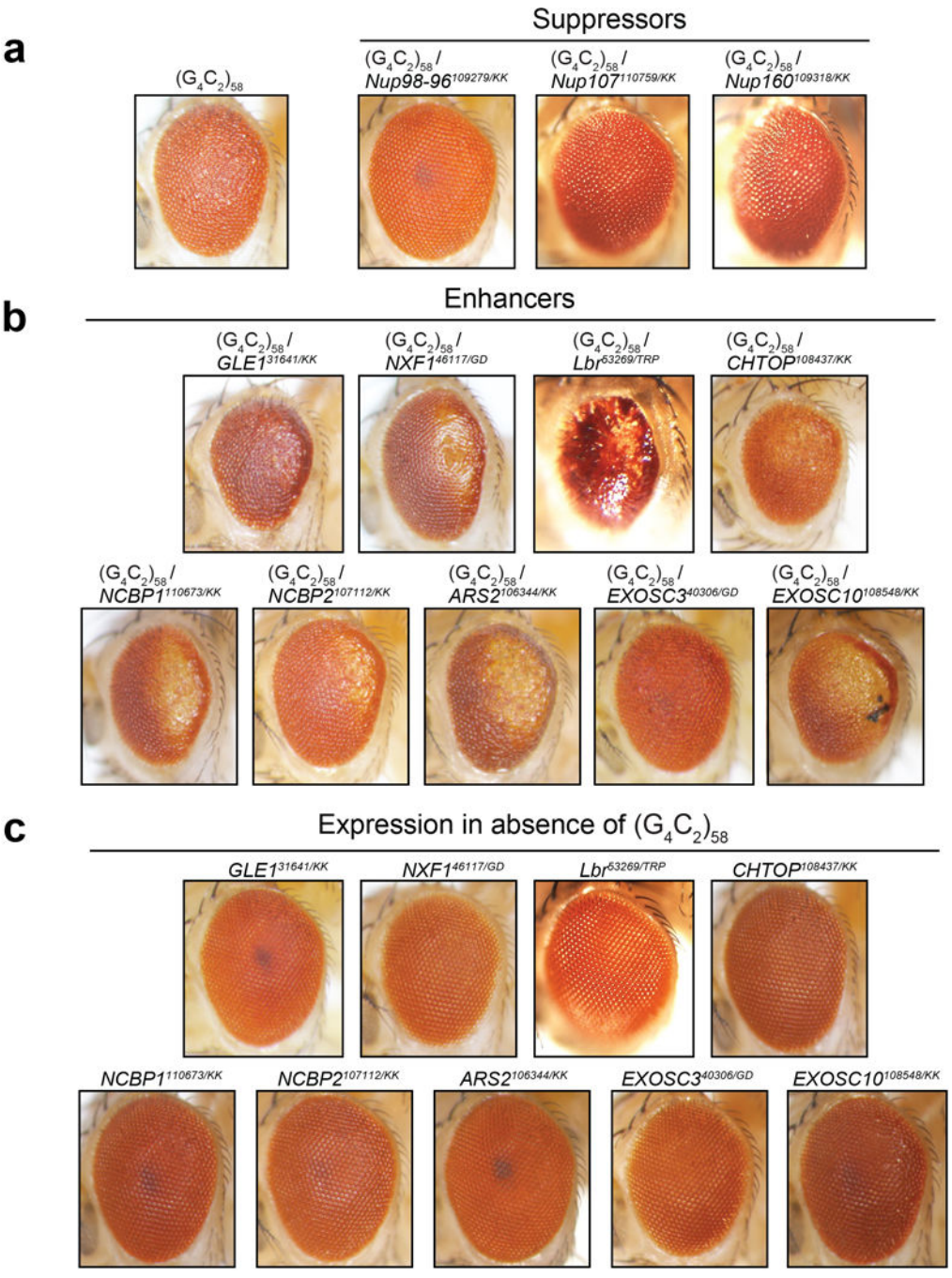

Extended Data Figure 5. Phenotypes of additional suppressors and enhancers of G_4C_2-58

a, Phenotypes demonstrating suppression of the G_4C_2-58 rough eye phenotype by RNAi knock down of identified genes. **b**, Phenotypes demonstrating enhancement of the G_4C_2-58 rough eye phenotype by RNAi knock down of identified genes. **c**, Knock down of identified modifier genes shows little or no phenotype in the absence of G_4C_2 repeat expression.

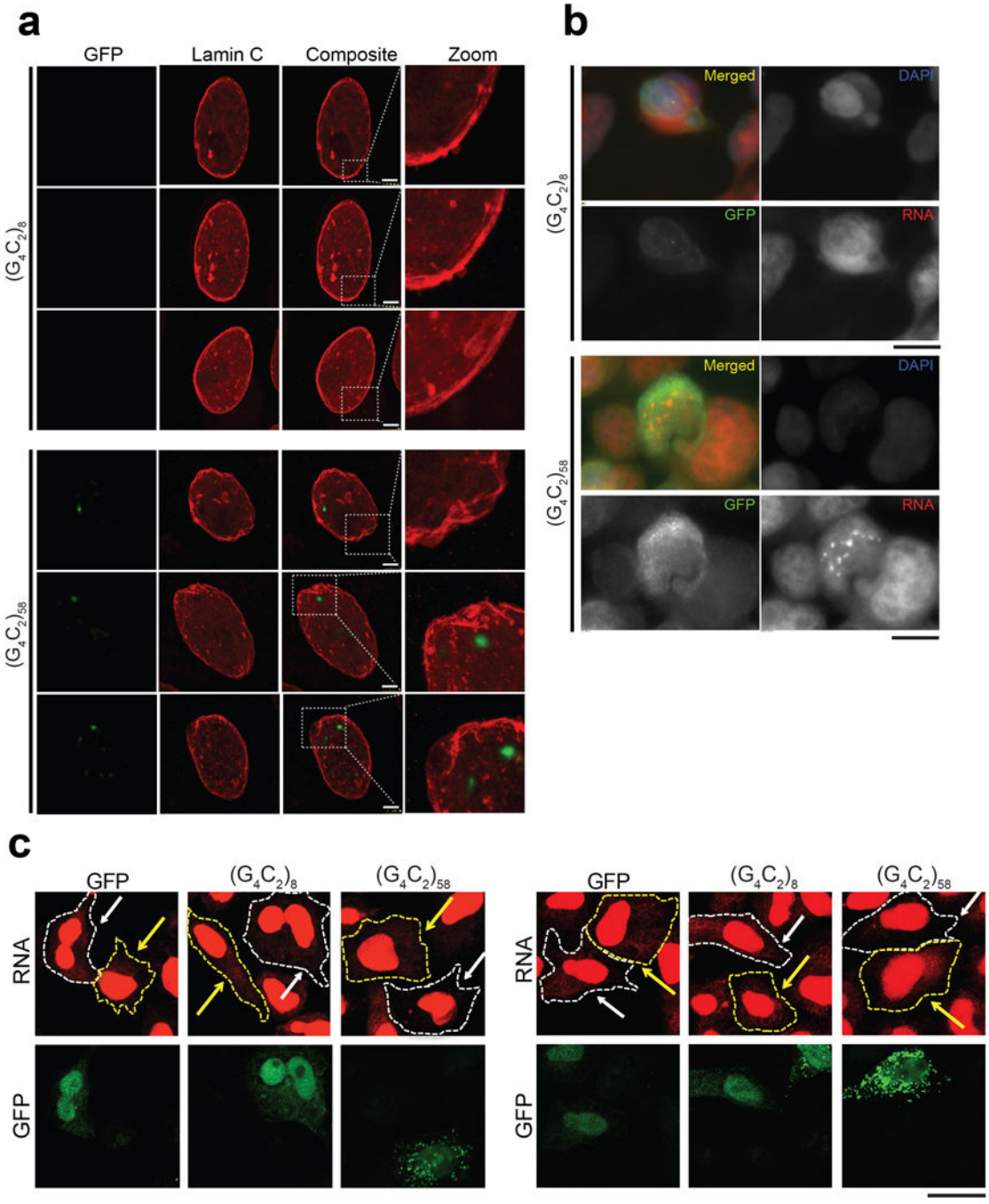

Extended Data Figure 6. Impairment of Nucleocytoplasmic shuttling in *Drosophila* and cultured human cell lines

a, G_4C_2-58 expression driven by *FKH-GAL4* causes an abnormal nuclear envelope as shown by Lamin C staining (bottom) in comparison to G_4C_2-8 (top). Scale bar: 10 μm. b, Transfection of 293T cells with G_4C_2-58 (bottom) but not G_4C_2-8 (top) leads to an increase in nuclear RNA puncta as visualized with a total RNA FISH probe. Non-transefected cells (absence of GFP signal) do not show an increase in nuclear RNA in either G_4C_2-8 or G_4C_2-58 transfected cell. Scale bars: 25 μm. **c**, Enlarged images showing slowed accumulation of newly synthesized RNA in the cytoplasm of HeLa cells expressing G_4C_2-58. Scale bar: 25 μm.

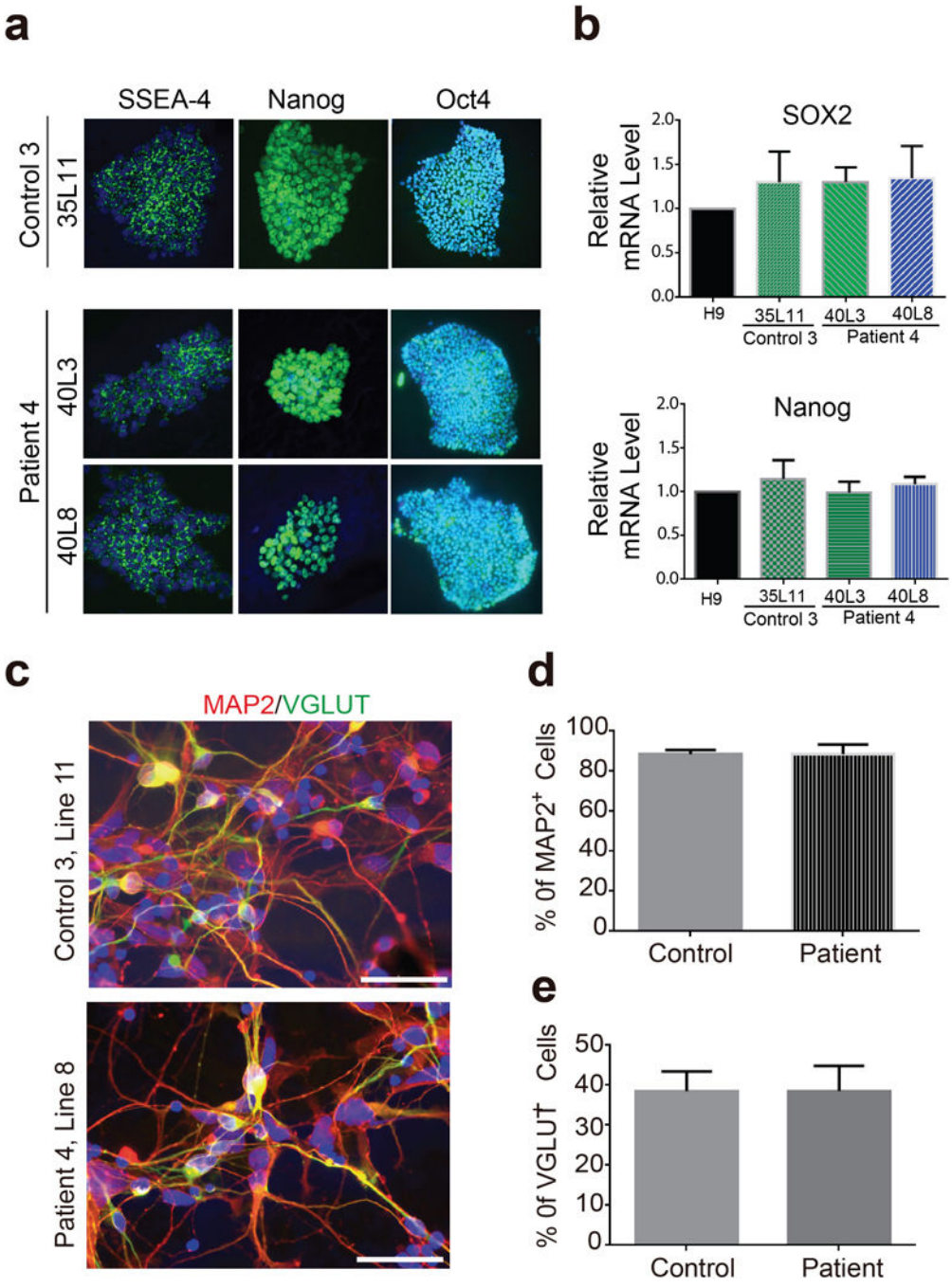

Extended Data Figure 7. Characterization of newly generated integration-free iPSCs lines

a, iPSC lines from a control subject (Line 11) and a G_4C_2 repeat expansion carrier (Line 3 and Line 8) express pluripotent markers SSEA-4, Nanog and Oct-4. Bars: 50 μm. **b**, qRT-PCR analysis ofexpression levels of pluripotent stem cell markers SOX2 and Nanog in these iPSCs lines showing no statistical differences between these lines and human embryonic stem cell line H9. **c**, After differentiation into cortical neurons about 90% of cells in these cultures are MAP2-positive neurons. **d**, Quantification of average percentage of MAP2-positive neurons and there is no difference between control and C9ORF72 cultures. **e**,

Quantification of average percentage of VGLUT-positive excitatory neurons among all neurons and there is no difference between control and C9ORF72 cultures. Scale bars in all panels: 50 mm.

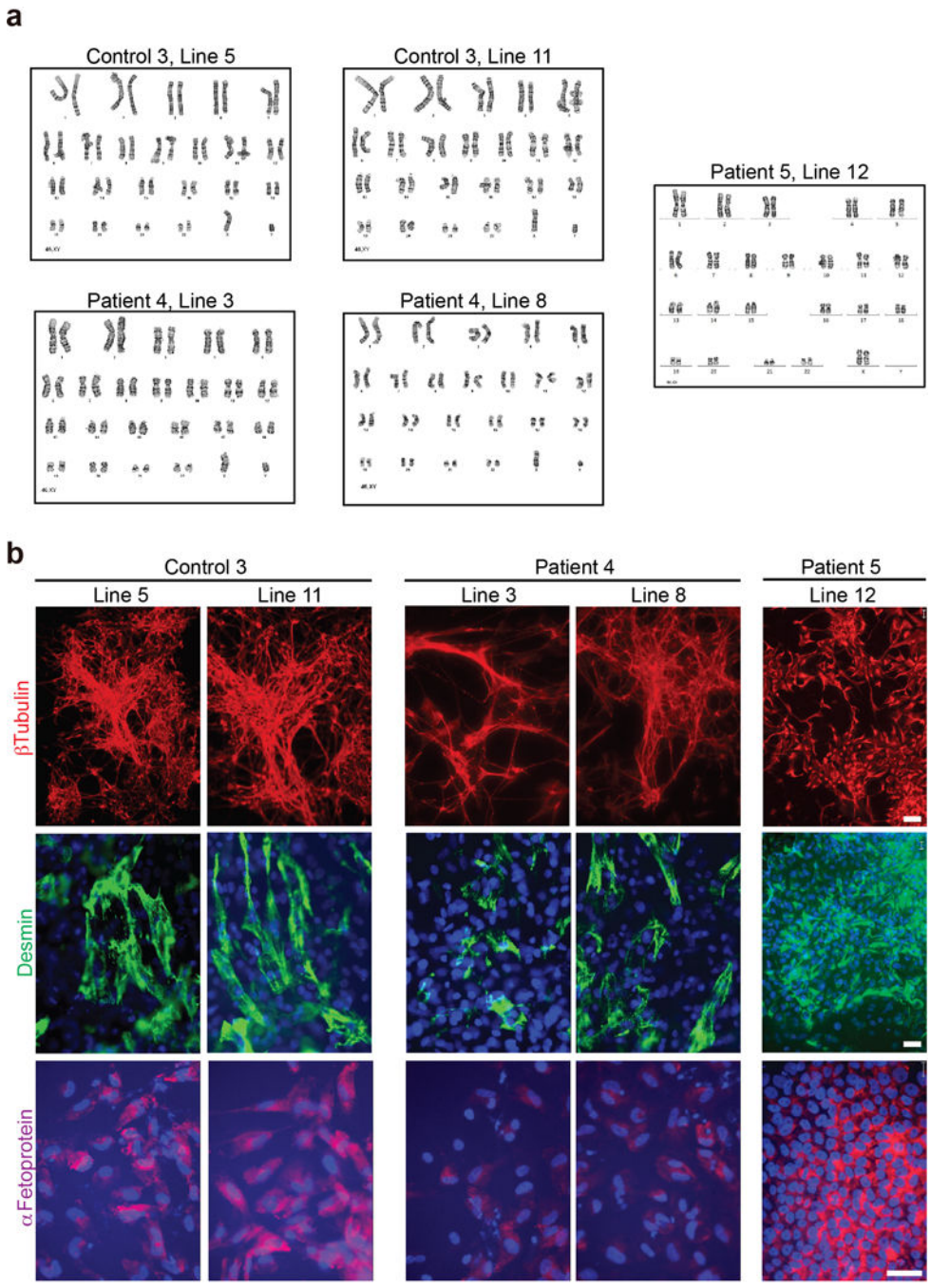

Extended Data Figure 8. Karyotyping analysis and pluripotency of newly generated iPSC lines

a, G-band staining showing a normal karyotype for all the lines analyzed. **b**, After *in vitro* spontaneous differentiation of control and C9 carrier iPSC lines, cells were staining for α-fetoprotein (AFP, endoderm), desmin (mesoderm), βIII-tubulin (ectoderm), and Hoechst

(nuclei). All lines showed differentiation towards derivates of three germ layers. Scale bars: 20 mm.

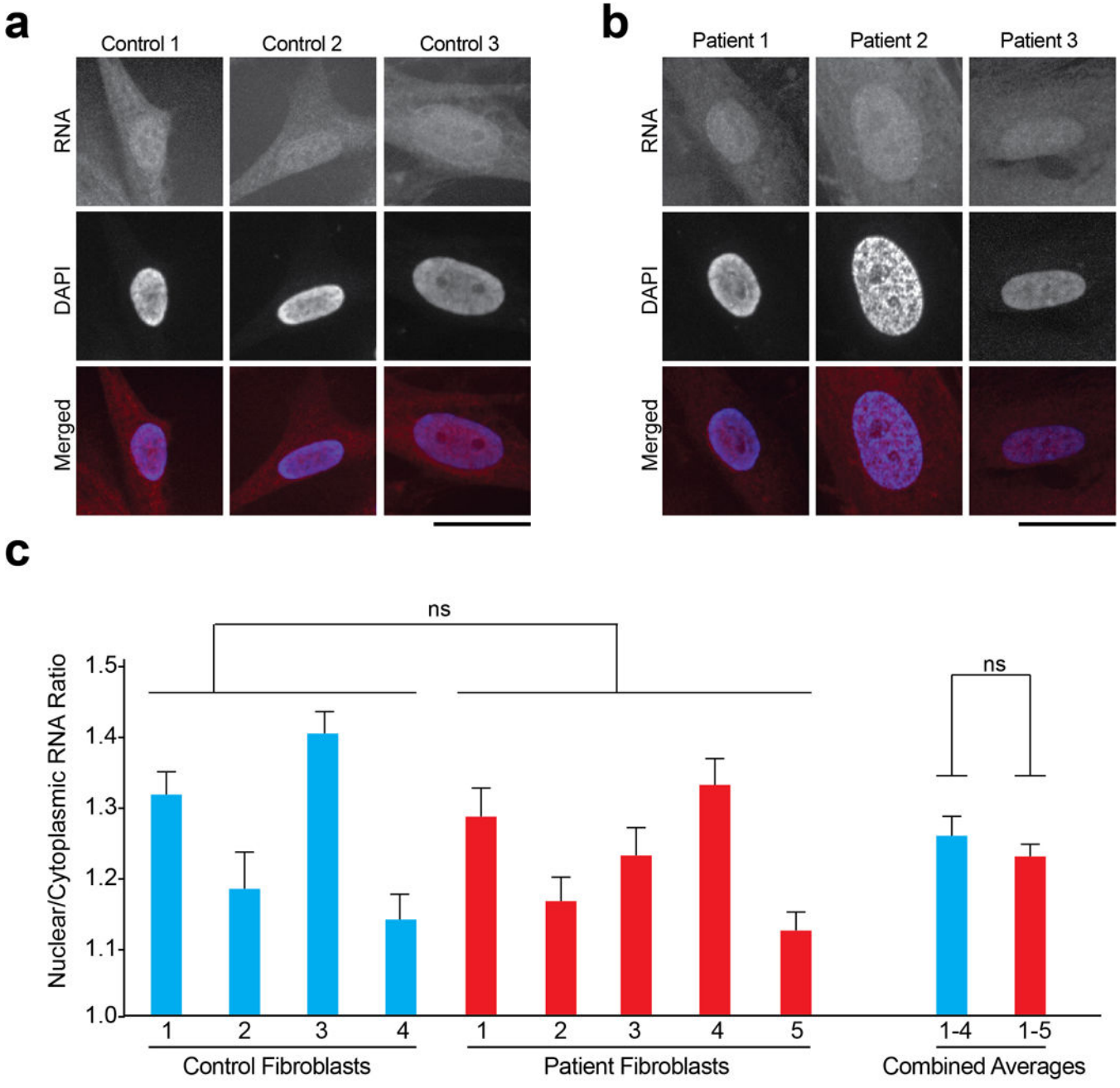

Extended Data Figure 9. Accumulation of nuclear RNA is not seen in fibroblasts derived from patients with G_4C_2 repeat expansion

a and **b**, Total cellular RNA was measured by FISH in fibroblasts derived from either control (**a**) subjects or patients (**b**) with G_4C_2 repeat expansion. Scale bars: 25 μm. **c**, Quantification shows no statistical difference in the observed nuclear to cytoplasmic RNA ratio in patient vs. control fibroblasts. n=16 for all lines.

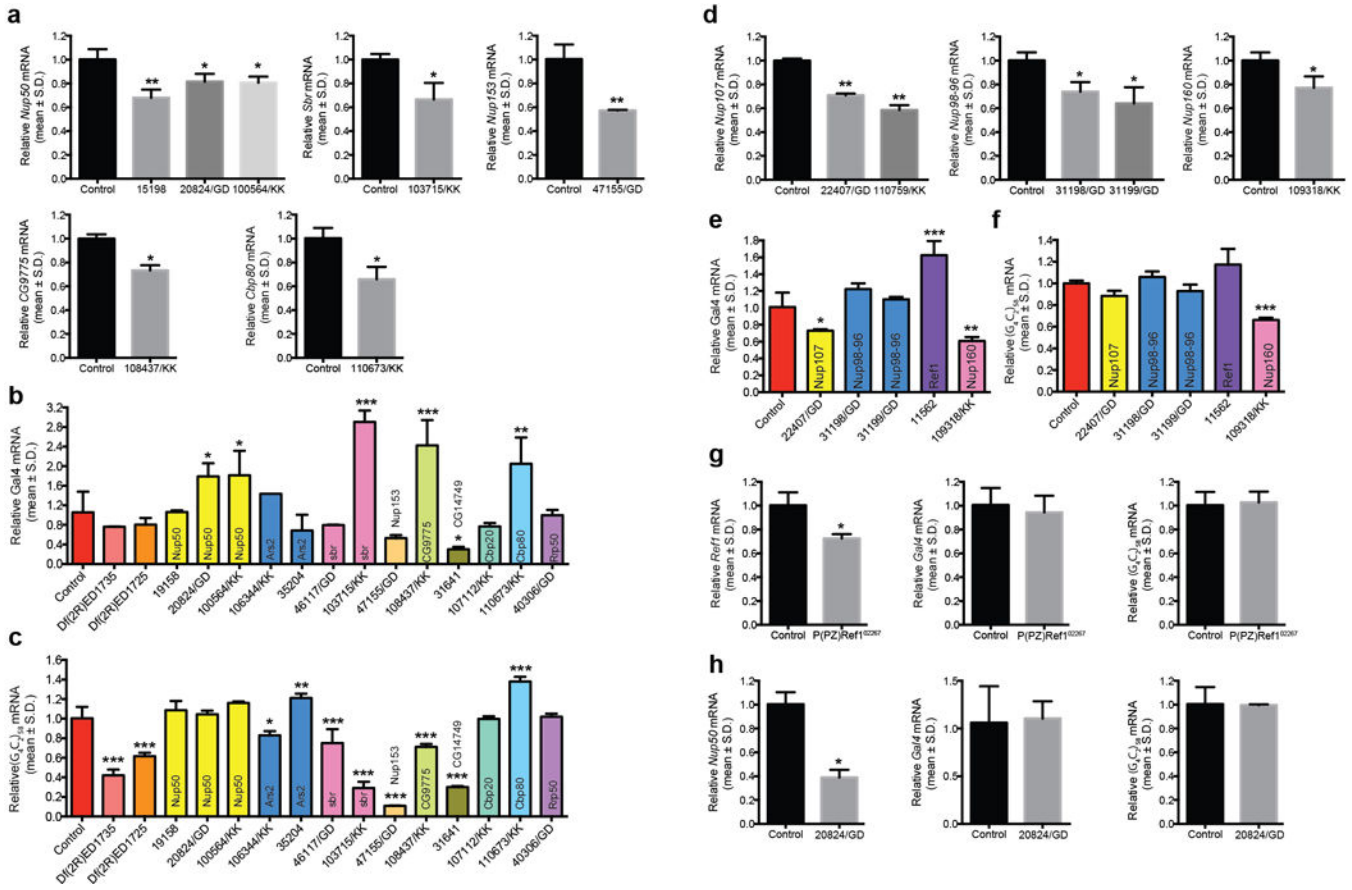

Extended Data Figure 10. qRT-PCR Analysis

a–f. qRT-PCR analysis demonstrating knockdown of selected modifiers in *Drosophila* eyes. mRNA levels of selected modifier (**a, d**), GAL4 (**b, e**), and G_4C_2-58 (**c, f**) assayed by qRT-PCR in progeny resulting from wild type (w1118), classical mutant allele or UAS-RNAi lines of selected modifiers mated with either *GMR-GAL4* or *GMR-GAL4/Cyo;UAS-G_4C_2-58-GFP/TM6* to induce knockdown of the selected gene. RNA was obtained from whole *Drosophila* head lysates. Gene expression levels are mean ± S.D., *p < 0.05, **p<0.01, ***p<0.001 by One Way ANOVA, Tukey's Post Hoc test. **g–h**. qRT-PCR analysis demonstrating knockdown of *Ref1* and nup50 in Salivary Gland. mRNA levels of selected modifier (left), GAL4 (middle), and G_4C_2-58 (right) assayed by qRT-PCR in progeny resulting from either P(PZ)*Ref1*02267 (**g**), or nup5020824/GD (**h**) mated with *FKH-GAL4,UAS-G_4C_2-58-GFP/TM6.* RNA was obtained from salivary gland lysates. Gene expression levels are mean ± S.D., *p < 0.05 by Student's t-test.

Supplementary Material

Refer to Web version on PubMed Central for supplementary material.

Acknowledgments

We thank the Bloomington *Drosophila* Stock Center, the VDRC Stock Center, Drs. K. McKim and E. Baehrecke for fly lines, Dr. V. Budnik for Lamin C antibody, as well as the Cell and Tissue Imaging Core at St. Jude Children's

Research Hospital and the University of Massachusetts Medical School Confocal Core for assistance. This work was supported by grants from Target ALS, The Packard Center for ALS Research at the Johns Hopkins University, and the ALS Association to F.B.G. and J.P.T., and ALS Therapy Alliance, NIH (N079725) to F.B.G and NIH (NS079725 and AG019724) to B.L.M.

References

1. DeJesus-Hernandez M, et al. Expanded GGGGCC hexanucleotide repeat in noncoding region of C9ORF72 causes chromosome 9p-linked FTD and ALS. Neuron. 2011; 72:245–256. doi:S0896-6273(11)00828-2[pii]10.1016/j.neuron.2011.09.011. [PubMed: 21944778]
2. Renton AE, et al. A hexanucleotide repeat expansion in C9ORF72 is the cause of chromosome 9p21-linked ALS-FTD. Neuron. 2011; 72:257–268. DOI: 10.1016/j.neuron.2011.09.010 [PubMed: 21944779]
3. Mizielinska S, et al. C9orf72 repeat expansions cause neurodegeneration in Drosophila through arginine-rich proteins. Science. 2014; 345:1192–1194. DOI: 10.1126/science.1256800 [PubMed: 25103406]
4. Xu Z, et al. Expanded GGGGCC repeat RNA associated with amyotrophic lateral sclerosis and frontotemporal dementia causes neurodegeneration. Proc Natl Acad Sci U S A. 2013; 110:7778–7783. DOI: 10.1073/pnas.1219643110 [PubMed: 23553836]
5. Kwon I, et al. Poly-dipeptides encoded by the C9orf72 repeats bind nucleoli, impede RNA biogenesis, and kill cells. Science. 2014; 345:1139–1145. DOI: 10.1126/science.1254917 [PubMed: 25081482]
6. Wen X, et al. Antisense proline-arginine RAN dipeptides linked to C9ORF72-ALS/FTD form toxic nuclear aggregates that initiate in vitro and in vivo neuronal death. Neuron. 2014; 84:1213–1225. DOI: 10.1016/j.neuron.2014.12.010 [PubMed: 25521377]
7. Makise M, et al. The Nup153-Nup50 protein interface and its role in nuclear import. J Biol Chem. 2012; 287:38515–38522. DOI: 10.1074/jbc.M112.378893 [PubMed: 23007389]
8. Cesario J, McKim KS. RanGTP is required for meiotic spindle organization and the initiation of embryonic development in Drosophila. J Cell Sci. 2011; 124:3797–3810. DOI: 10.1242/jcs.084855 [PubMed: 22100918]
9. Reed R. Coupling transcription, splicing and mRNA export. Curr Opin Cell Biol. 2003; 15:326–331. [PubMed: 12787775]
10. Viphakone N, et al. TREX exposes the RNA-binding domain of Nxf1 to enable mRNA export. Nat Commun. 2012; 3:1006. [PubMed: 22893130]
11. Zhou Z, et al. The protein Aly links pre-messenger-RNA splicing to nuclear export in metazoans. Nature. 2000; 407:401–405. DOI: 10.1038/35030160 [PubMed: 11014198]
12. Chang CT, et al. Chtop is a component of the dynamic TREX mRNA export complex. The EMBO journal. 2013; 32:473–486. DOI: 10.1038/emboj.2012.342 [PubMed: 23299939]
13. Wan J, et al. Mutations in the RNA exosome component gene EXOSC3 cause pontocerebellar hypoplasia and spinal motor neuron degeneration. Nat Genet. 2012; 44:704–708. DOI: 10.1038/ng.2254 [PubMed: 22544365]
14. Cheng H, et al. Human mRNA export machinery recruited to the 5 end of mRNA. Cell. 2006; 127:1389–1400. DOI: 10.1016/j.cell.2006.10.044 [PubMed: 17190602]
15. Boehmer T, Enninga J, Dales S, Blobel G, Zhong H. Depletion of a single nucleoporin, Nup107, prevents the assembly of a subset of nucleoporins into the nuclear pore complex. Proc Natl Acad Sci U S A. 2003; 100:981–985. DOI: 10.1073/pnas.252749899 [PubMed: 12552102]
16. Vasu S, et al. Novel vertebrate nucleoporins Nup133 and Nup160 play a role in mRNA export. J Cell Biol. 2001; 155:339–354. DOI: 10.1083/jcb.200108007 [PubMed: 11684705]
17. Walther TC, et al. The conserved Nup107-160 complex is critical for nuclear pore complex assembly. Cell. 2003; 113:195–206. [PubMed: 12705868]
18. Murphy R, Wente SR. An RNA-export mediator with an essential nuclear export signal. Nature. 1996; 383:357–360. DOI: 10.1038/383357a0 [PubMed: 8848052]
19. Nousiainen HO, et al. Mutations in mRNA export mediator GLE1 result in a fetal motoneuron disease. Nat Genet. 2008; 40:155–157. DOI: 10.1038/ng.2007.65 [PubMed: 18204449]

20. Kaneb HM, et al. Deleterious mutations in the essential mRNA metabolism factor, hGle1, in amyotrophic lateral sclerosis. Hum Mol Genet. 2015; 24:1363–1373. DOI: 10.1093/hmg/ddu545 [PubMed: 25343993]
21. Han SS, Williams LA, Eggan KC. Constructing and deconstructing stem cell models of neurological disease. Neuron. 2011; 70:626–644. DOI: 10.1016/j.neuron.2011.05.003 [PubMed: 21609821]
22. van Blitterswijk M, DeJesus-Hernandez M, Rademakers R. How do C9ORF72 repeat expansions cause amyotrophic lateral sclerosis and frontotemporal dementia: can we learn from other noncoding repeat expansion disorders? Curr Opin Neurol. 2012; 25:689–700. DOI: 10.1097/WCO.0b013e32835a3efb [PubMed: 23160421]
23. Almeida S, et al. Modeling key pathological features of frontotemporal dementia with C9ORF72 repeat expansion in iPSC-derived human neurons. Acta Neuropathol. 2013; 126:385–399. DOI: 10.1007/s00401-013-1149-y [PubMed: 23836290]
24. Zhang Z, et al. Downregulation of microRNA-9 in iPSC-derived neurons of FTD/ALS patients with TDP-43 mutations. PLoS One. 2013; 8:e76055. [PubMed: 24143176]
25. Sareen D, et al. Targeting RNA foci in iPSC-derived motor neurons from ALS patients with a C9ORF72 repeat expansion. Sci Transl Med. 2013; 5:208ra149.
26. Cronshaw JM, Matunis MJ. The nuclear pore complex: disease associations and functional correlations. Trends Endocrinol Metab. 2004; 15:34–39. [PubMed: 14693424]
27. Savas JN, Toyama BH, Xu T, Yates JR 3rd, Hetzer MW. Extremely long-lived nuclear pore proteins in the rat brain. Science. 2012; 335:942. [PubMed: 22300851]
28. Mor A, White MA, Fontoura BM. Nuclear trafficking in health and disease. Curr Opin Cell Biol. 2014; 28:28–35. DOI: 10.1016/j.ceb.2014.01.007 [PubMed: 24530809]
29. Bonnet A, Palancade B. Regulation of mRNA trafficking by nuclear pore complexes. Genes (Basel). 2014; 5:767–791. DOI: 10.3390/genes5030767 [PubMed: 25184662]
30. Zhang YJ, et al. Aggregation-prone c9FTD/ALS poly(GA) RAN-translated proteins cause neurotoxicity by inducing ER stress. Acta Neuropathol. 2014; 128:505–524. DOI: 10.1007/s00401-014-1336-5 [PubMed: 25173361]
31. Kim NC, et al. VCP is essential for mitochondrial quality control by PINK1/Parkin and this function is impaired by VCP mutations. Neuron. 2013; 78:65–80. DOI: 10.1016/j.neuron.2013.02.029 [PubMed: 23498974]
32. Smith R, Taylor JP. Dissection and imaging of active zones in the Drosophila neuromuscular junction. Journal of visualized experiments: JoVE. 2011
33. Gendron TF, et al. Antisense transcripts of the expanded C9ORF72 hexanucleotide repeat form nuclear RNA foci and undergo repeat-associated non-ATG translation in c9FTD/ALS. Acta neuropathologica. 2013; 126:829–844. DOI: 10.1007/s00401-013-1192-8 [PubMed: 24129584]
34. Ash PE, et al. Unconventional translation of C9ORF72 GGGGCC expansion generates insoluble polypeptides specific to c9FTD/ALS. Neuron. 2013; 77:639–646. DOI: 10.1016/j.neuron.2013.02.004 [PubMed: 23415312]
35. Almeida S, et al. Induced pluripotent stem cell models of deficient frontotemporal dementia uncover specific reversible neuronal defects. Cell Rep. 2012; 2:789–798. DOI: 10.1016/j.celrep.2012.09.007 [PubMed: 23063362]
36. Okita K, et al. A more efficient method to generate integration-free human iPS cells. Nat Methods. 2011; 8:409–412. DOI: 10.1038/nmeth.1591 [PubMed: 21460823]

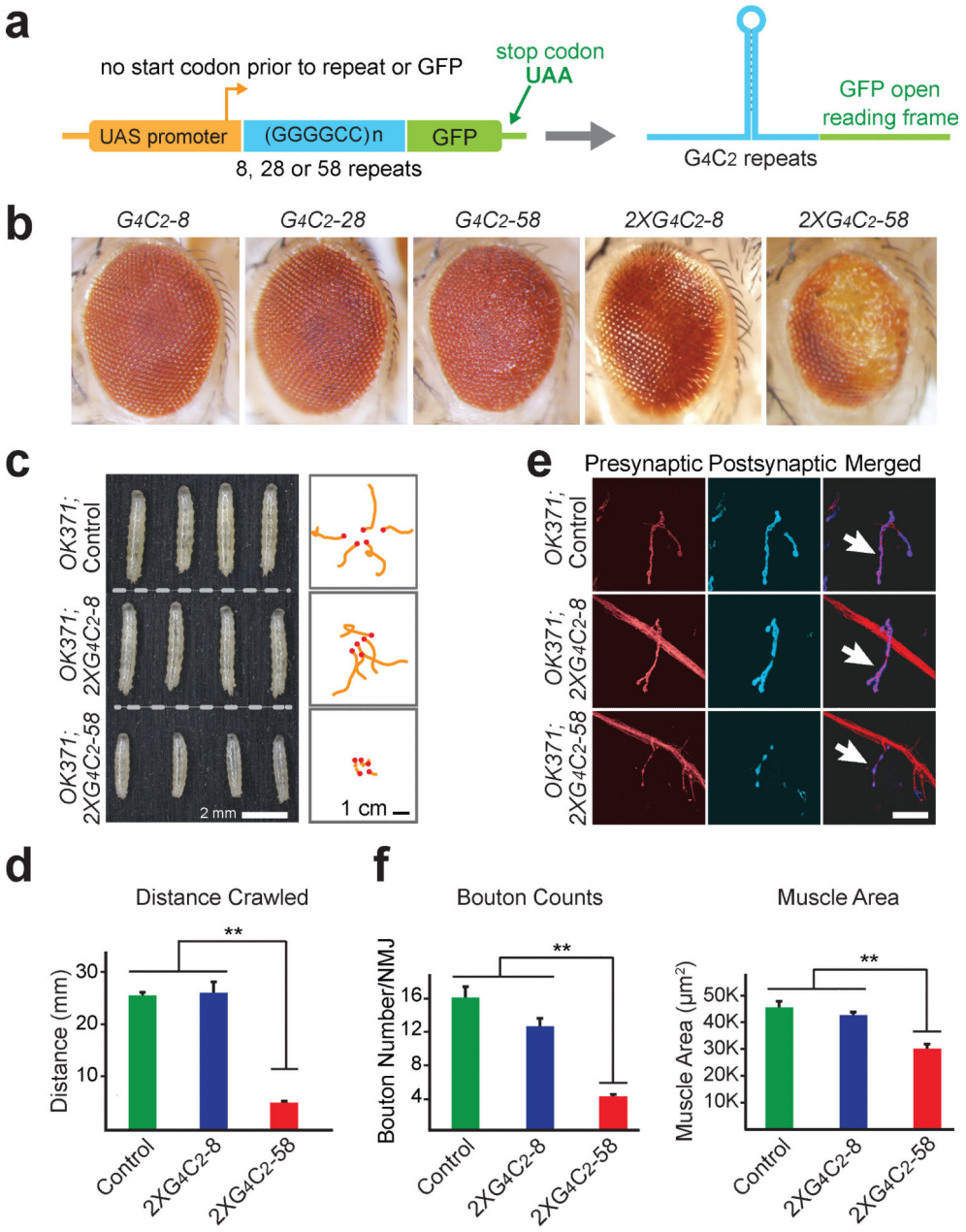

Figure 1. G_4C_2 repeats induces length- and dosage-dependent degeneration in *Drosophila*

a, Constructs expressing 8, 28, or 58 copies of G_4C_2 repeats. **b**, G_4C_2-58 causes a rough eye phenotype. **c**, Two copies of G_4C_2-58 expressed in motor neurons results in a decrease in larval size (left panel) and locomotor activity (right panel). **d**, Quantification of the distance traveled by larvae expressing repeats in motor neurons. Values are mean ± s.e.m., n = 3 trials, ** $p < 0.01$, by One Way ANOVA, Tukey's Post Hoc test. **e**, Expression of two copies of G_4C_2-58 in motor neurons reduces bouton number. Scale bar: 25 μm. **f**, Quantification of bouton number and muscle size in larvae expressing G_4C_2 repeats. Values are mean ± s.e.m., n = 6, ** $p < 0.01$, by One Way ANOVA, Tukey's Post Hoc test.

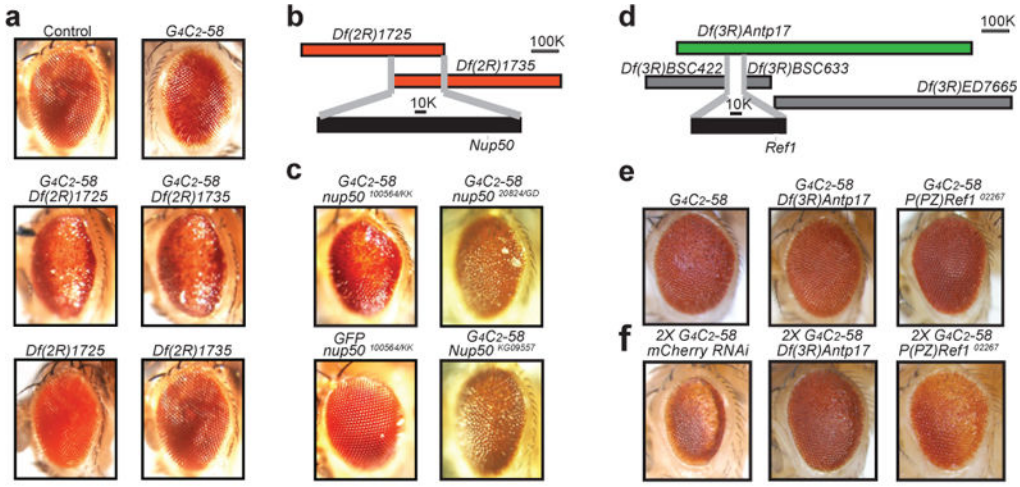

g

Gene Name	Human Ortholog	Modification	Biological Function	Protein Localization in cell	Stock ID
Nup50	*NUP50*	Enhancer	Nuclear Import	Nuclear Pore	VDRC: 20824_GD, 100564_KK; Classical: 15198
Nup153	*NUP153*	Enhancer	Nuclear Import	Nuclear Pore	VDRC: 47155_GD, 107750_KK
Trn	*TNPO1*	Enhancer	Nuclear Import	Nucleus / Cytoplasm	VDRC: 105181_KK
Crm1	*XPO1*	Enhancer	Nuclear Export	Nucleus / Cytoplasm	TRP: 31353
Ran	*RAN*	Enhancer	Nuclear Import / Export	Nucleus / Cytoplasm	Transgenic T24N
LBR	*LBR*	Enhancer	Nuclear Membrane Structure	Nuclear Membrane	TRP:53269
Nup107	*NUP107*	Suppressor	Nuclear Import / Export	Nuclear Pore	VDRC: 22407_GD, 110759_KK
Nup160	*NUP160*	Suppressor	Nuclear Import / Export	Nuclear Pore	VDRC: 109318_KK
Nup98-96	*NUP98*	Suppressor	Nuclear Import / Export	Nuclear Pore	VDRC: 31198_GD, 31199_GD, 109279_KK
CG9775	*CHTOP*	Enhancer	RNA Export	Nucleus	VDRC: 108437_KK
sbr	*NXF1*	Enhancer	RNA Export	Nucleus	TRP:28924; VDRC: 46117_GD, 103715_KK
CG14749	*GLE1*	Enhancer	RNA Export	Nucleus	TRP:31641
Cbp80	*NCBP1*	Enhancer	Cap Binding Protein	RNA 5' Cap	VDRC: 22332_GD, 110673_KK
Cbp20	*NCBP2*	Enhancer	Cap Binding Protein	RNA 5' Cap	VDRC: 107112_KK
Ars2	*ARS2*	Enhancer	Cap Binding Protein	RNA 5' Cap	TRP: 32844, 35204; VDRC: 106344_KK
Ref1	*ALYREF*	Suppressor	Couples Transcription to Export	Nucleus	Classical: 11562
Rrp40	*EXOSC3*	Enhancer	RNA Degradation	Exosome	VDRC: 40306_GD
Rrp6	*EXOSC10*	Enhancer	RNA Degradation	Exosome	VDRC: 108548_KK

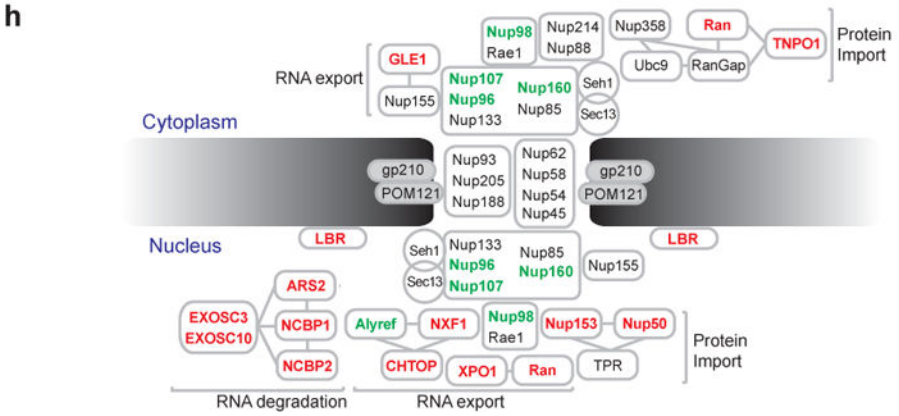

Figure 2. Genetic screen identifies multiple modifiers of G_4C_2-58 toxicity in the nucleocytoplasmic transport pathway

a, G_4C_2-58 expression driven by *GMR-GAL4* causes a rough eye phenotype (top right) that was enhanced by either *Df(2R)1725/+* or *Df(2R)1735/+*(middle). **b**, Overlapping genomic region of deficiency lines *Df(2R)1725* or *Df(2R)1735*. **c**, RNAi knockdown (*Nup50*$^{20824/GD}$ and *Nup50*$^{100564/KK}$) and a genetic allele (*Nup50*^{KG09557}) identify *Nup50* as an enhancer. **d**, The deficiency *Df(3R)Antp17* (green) but not others (grey) suppressed the G_4C_2-58 eye phenotype. **e and f**, Identification of *Ref* as a suppressor. **g**, Table summarizing modifier

genes and their known functions. **h**, Suppressors (green) and enhancers (red) of G_4C_2-58 toxicity in the nucleocytoplasmic trafficking pathway.

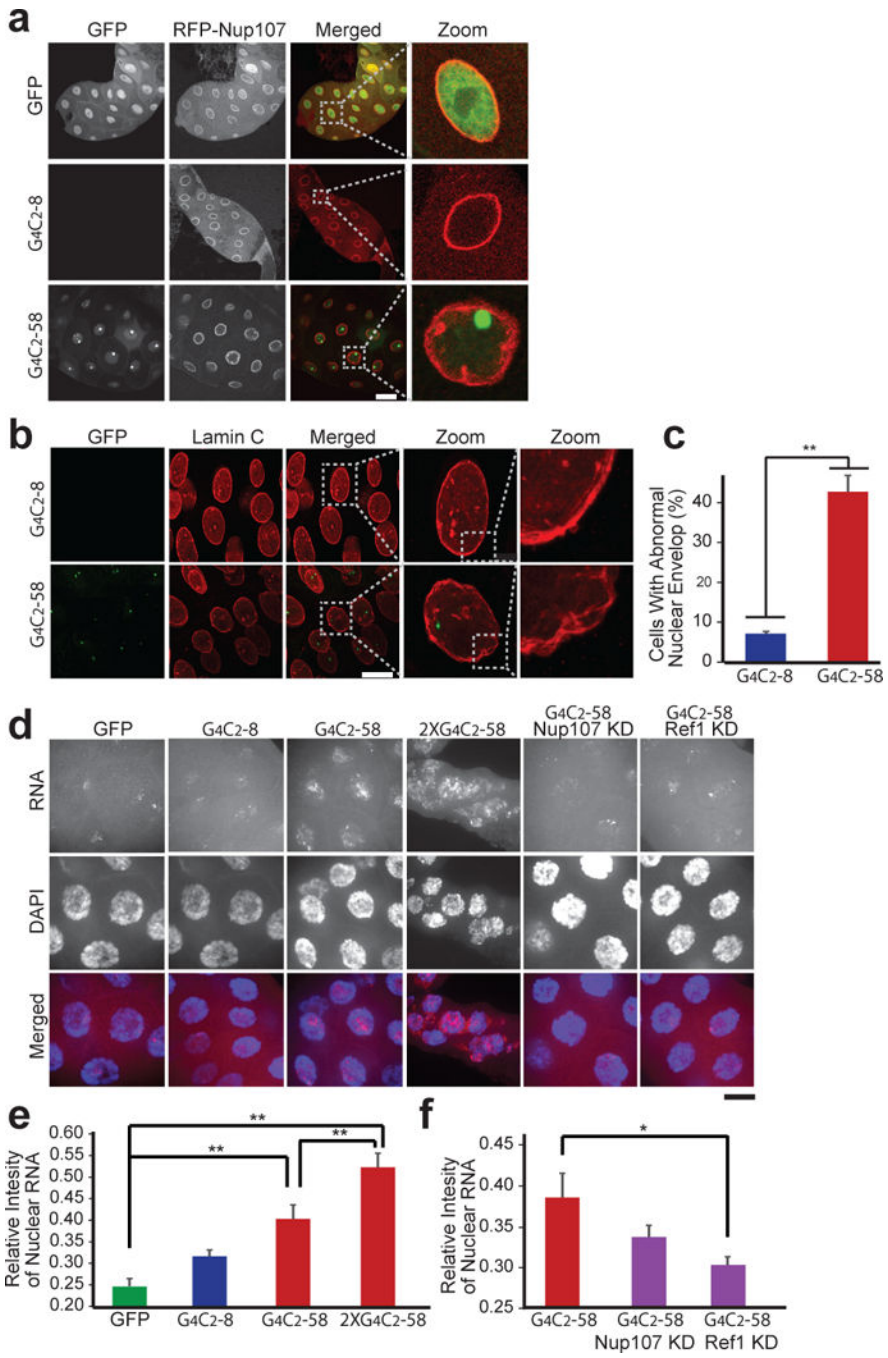

Figure 3. *Drosophila* salivary gland cells expressing G_4C_2-58 exhibit nuclear envelope abnormalities and accumulation of nuclear RNA

a, The effect of G_4C_2-58 expression on Nup107 localization. Scale bar: 50 μm. **b**, G_4C_2-58 expression causes abnormal nuclear envelope morphology. Scale bar: 50 μm. **c**, Quantification of the frayed nuclear envelope phenotype in cells expressing either G_4C_2-8 (n = 251) or G_4C_2-58 (n = 127). Values are mean ± s.e.m., ** $p < 0.001$ by Student's t test. **d**, Accumulation of total nuclear RNA relative to cytoplasmic RNA (red). Knockdown of *Ref1* led to a partial rescue of nuclear RNA accumulation. Scale bar: 25 μm. **e and f**,

Quantification of relative intensity of total nuclear RNA vs. cytoplasmic RNA. Values are mean ± s.e.m., n = 30 cells, * $p < 0.01$, ** $p < 0.001$ by One Way ANOVA, Tukey's Post Hoc test.

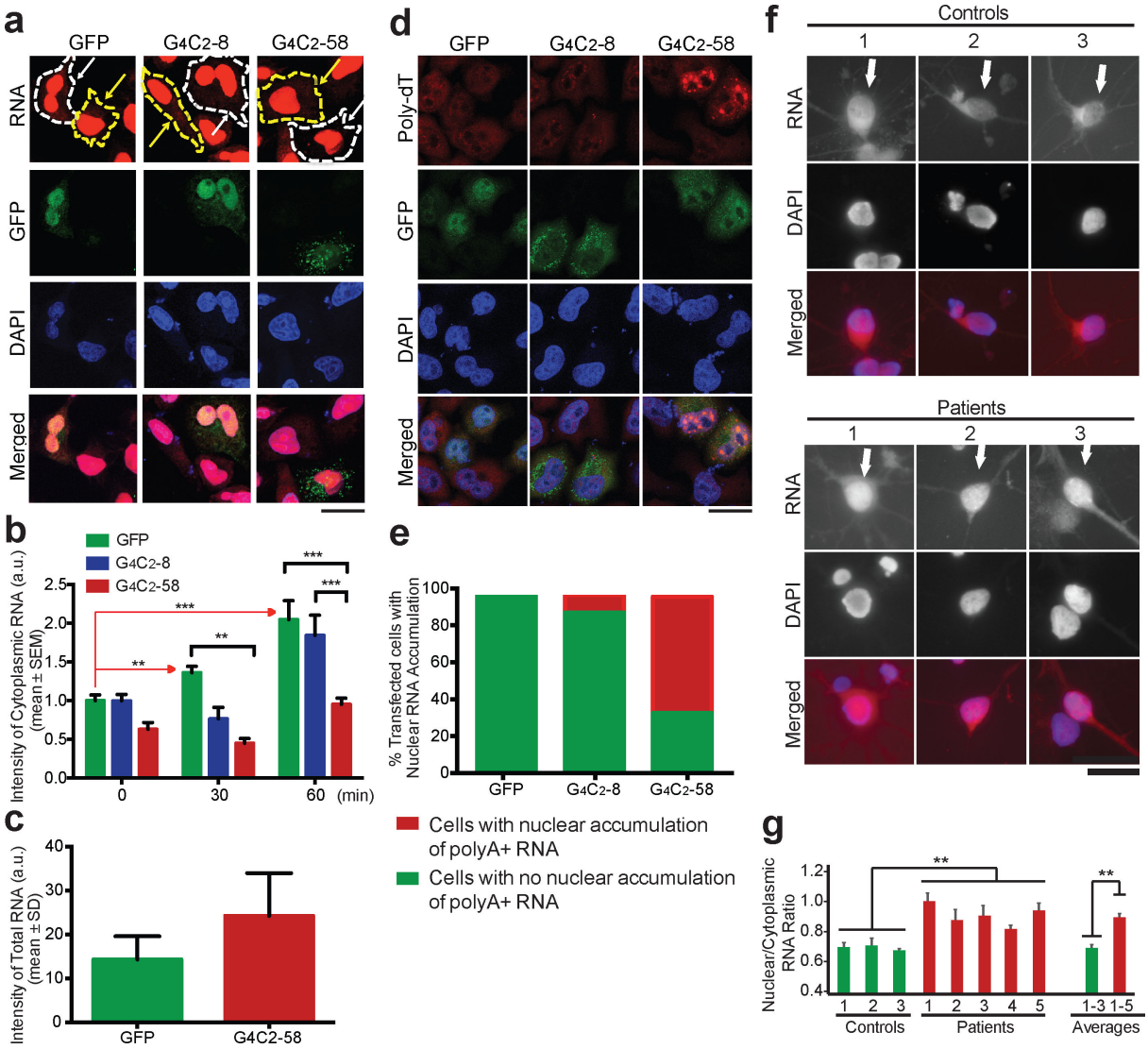

Figure 4. Accumulation of nuclear RNA in human cells expressing G_4C_2 repeat expansion

a, Reduced accumulation of newly synthesized RNA in the cytoplasm of cells transfected with G_4C_2-58 (white arrows) (imaged at 60 min). Yellow arrows: untransfected cells. **b**, Quantification of cytoplasmic RNA intensity following metabolic labeling of newly synthesized RNA (0 min: n > 24, 30 min: n > 7, 60 min: n > 25). ** $p < 0.01$, *** $p < 0.001$ by One Way ANOVA, Tukey's Post Hoc test. **c**, Total RNA intensity following labeling of newly synthesized RNA at time point 0 min. **d**, PolyA$^+$ RNA was measured by FISH in transiently transfected HeLa cells. Scale bar: 50 μm. **e**, Quantification of cells containing polyA$^+$ RNA puncta, n = 30 cells per condition. **f**, Total cellular RNA in 2-month old iPSCs-derived cortical neurons. Scale bar: 25 μm. **g**, Quantification of the cytoplasmic RNA ratio in patient cortical neurons vs. controls. Values are mean ± s.e.m., n > 15 cells per line, ** $p < 0.01$ by Student's t test.